Phase diagrams of Kitaev models for arbitrary magnetic field orientations

F. Yılmaz* and A. P. Kampf
Theoretical Physics III, Center for Electronic Correlations and Magnetism, Institute of Physics, University of Augsburg, Augsburg 86135, Germany

S. K. Yip
Institute of Physics, Academia Sinica, Taipei 115, Taiwan and Institute of Atomic and Molecular Sciences, Academia Sinica, Taipei 115, Taiwan

(Received 15 February 2022; revised 24 August 2022; accepted 26 August 2022; published 12 October 2022)

The Kitaev model is an exactly solvable quantum spin model within the language of constrained real fermions. In spite of numerous studies for magnetic fields along special orientations, there is a limited amount of knowledge on the complete field-angle characterization, which can provide valuable information on the existence of fractionalized excitations. For this purpose, we first study the pure ferromagnetic and antiferromagnetic Kitaev models for arbitrary external magnetic field directions via a mean-field theory, showing that there are many topological phases with different (or zero) Chern numbers, depending on the magnetic field strength and orientations. However, a realistic description of the candidate Kitaev materials, within the edge-sharing octahedra paradigm, requires additional coupling terms, including a large off-diagonal term Γ along with possible anisotropic corrections Γ_p. It is therefore not sufficient to rely on the topological properties of the bare Kitaev model as the basis for the observed thermal Hall-conductivity signals, and an understanding of these extended Kitaev models with a complete field response is demanded. Starting from the zero-field phase diagram of K-Γ-Γ_p models, we identify, besides the Kitaev spin liquid phase, antiferromagnetic zigzag, ferromagnetic phases, as well as an unusual Kitaev(-Γ) spin liquid phase. The magnetic field response of these phases for arbitrary field orientations provides a remarkably rich phase diagram. For an extended parameter range and just above the critical field where the zigzag phase is suppressed, there is an intermediate phase region with suppressed energy gaps and substantial spin fractionalization. To comply our findings with experiments, we also reproduce a large asymmetry in the extent of this intermediate phases specifically for the two different field directions $\theta = \pm 60^o$ with respect to the normal to the plane of the honeycomb lattice.

DOI: 10.1103/PhysRevResearch.4.043024

I. INTRODUCTION

The Kitaev model is an exactly solvable [1] quantum spin model with fractionalized excitations within the family of spin liquid models. Candidate materials for its $J_{\rm eff} = 1/2$ ferromagnetic (F) realization are the iridates X_2IrO_3 (X: Li [2,3], Na [4–9]), and α-$RuCl_3$ [10–25]. Recently, there is a growing interest in the search of additional materials [26–28] with perhaps antiferromagnetic (AF) Kitaev type couplings such as in $Na_3Co_2SbO_6$-$Na_2Co_2TeO_6$ [29] and theoretical studies focusing on f-electron based rare-earth oxides [30]. These quantum magnets are acclaimed to have a significantly large Kitaev type spin-spin coupling. Detailed analyses of the underlying physics and the material characteristics have been summarized in numerous reviews [31–37].

The Kitaev model is defined on a honeycomb lattice with highly anisotropic Ising type exchange couplings at each bond direction,

$$H_K = \sum_{\langle ij \rangle}^{\alpha-\text{bond}} K^\alpha S_i^\alpha S_j^\alpha, \tag{1}$$

where the sublattices A and B are denoted with site index i and j respectively. It can host anyonic excitations within the real fermion language [1]. In this approach, each of the Pauli operators is replaced by two composite Majorana fermions $\sigma_j^\alpha = ib_j^\alpha c_j$, $\alpha \in \{x, y, z\}$ with the local constraint $D_j = b_j^x b_j^y b_j^z c_j = 1$ at site j. The basic theoretical work in materializing such an exotic model relies on the Jackeli-Khaliullin mechanism [38,39]. The effective Hamiltonians for transition metals are coupled with additional (extended) edge-sharing [40,41] octahedral ligands. The destructive interference between different exchange paths via ligands can eliminate the dominant Heisenberg exchange coupling in the effective spin Hamiltonian for transition metals. Thereby the additional Kitaev and other off-diagonal terms become dominant terms. There is also the additional proposition to tune the magnitude of each term by Floquet driving [42,43]. Eventually, most of the recent work has been allocated to the theoretical [38,44–47] and experimental investigation of the candidate materials. Experimental data suggest that it is

*firat.yilmaz@uni-a.de

highly likely for the candidate materials to have a spin-liquid ground state (GS) for intermediate magnetic field strengths. This is inferred in particular through bulk probes such as the continuum of excitations in neutron-scattering experiments [48] and thermodynamic measurements such as the field-angle dependence of the specific heat [49]. A significant amount of work has also focused on alternative explanations to a spin-liquid scenario such as chiral conventional quasiparticles [50–53] or beyond-Kitaev model spin liquids [54]. In all approaches, the anti/ferromagnetic Kitaev term has to be supplemented by additional interactions for a realistic material specific modeling. Depending on their relative strengths, the direct relation between the thermal Hall coefficient and the Kitaev interaction becomes obscure.

The thermal conductivity measurements has been recognized as a useful tool to rule in/out a topological Kitaev spin-liquid due to their charge neutral energy transport. In particular, a Kitaev spin liquid in a finite magnetic field is proposed to host a half-quantized neutral edge current as its distinct signature [1]. In an applied magnetic field, a gapless, topologically trivial Kitaev liquid can turn into a gapped, topologically nontrivial phase. Measurements [14–20] have shown that the magnetically ordered zigzag (ZZ) phase present in this material (as a result of spin interactions beyond the pure Kitaev model) can be suppressed by an external magnetic field, followed by a region with suppressed magnetization before the system enters into a field polarized (P) phase. In this intermediate field window, thermal Hall conductivity is anomalous [55,56]. Quantized thermal Hall conductance [57,58] has been reported in this region, giving support to a topologically nontrivial spin-liquid. Moreover, this quantized thermal Hall conductance, and an associated gap opening for the bulk excitations [49], can be generated by a pure in-plane magnetic field, lending further support to the topological origin of the field-induced topological phase. However, a recent experiment has revealed an unusual oscillation in the longitudinal thermal conductivity $\kappa_{\alpha\alpha}$ as a function of inverse magnetic field α-$RuCl_3$ [59] within the region of interest, which challenges some of the conclusions above. In this respect, a further characterization of this "intermediate phase" for arbitrary magnetic field strengths and directions could provide valuable information for the search of (non-)Abelian anyons.

In spite of numerous studies [60–68] along special field directions such as [001] and [111], there exists limited knowledge on the complete field-angle dependence of κ_{xy} in the Kitaev model itself. If the additional off-diagonal couplings are significant, it could be a naive approximation to relate thermal Hall coefficients to the pure Kitaev spin liquid. The studies on the candidate materials indicate the presence of a relatively large spin-orbit coupling Γ^α term, the off-diagonal coupling on the α-bond, $\sim\Gamma^\alpha(S_j^\beta S_l^\gamma + S_j^\gamma S_l^\beta)$ as well as the additional symmetry allowed Γ_p^α terms $\sim\Gamma_p^\alpha(S_j^\beta S_l^\alpha + S_j^\alpha S_l^\beta + S_j^\gamma S_l^\alpha + S_j^\alpha S_l^\gamma)$. Reference [69] has addressed this issue and also the magnetic field effects perturbatively, yet assuming a KSL GS. In this respect, it is crucial to clarify the effect of large $\Gamma \sim |K|$ [70,71] as well as arbitrary magnetic field orientations and strengths to understand the validity of existing results based on the putative F Kitaev GS. Naturally, an unbiased method is needed which takes into account spin ordering and spin liquid character on equal footing.

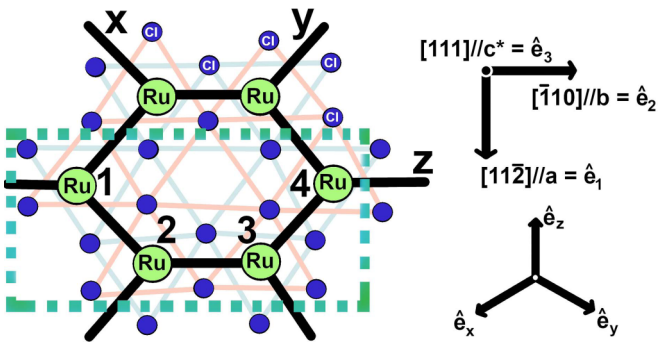

FIG. 1. The crystal structure of α-$RuCl_3$. The Ru atoms (green circles) form a honeycomb lattice (with black bonds) on the plane perpendicular to the crystallographic [111] direction, referred to as the c axis. The three bonds are labeled as x, y, and z. The Cl atoms form edge-sharing octahedra with two sublattices indicated by shaded blue and orange lines. For the Kitaev only models ($\Gamma = 0, \Gamma_p = 0$), we consider a unit cell contains two Ru sites connected by the z bond (indicated by site labels 2 and 3). For the Kitaev-Γ type models ($\Gamma \neq 0, \Gamma_p \neq 0$), a four-site unit cell is considered, as indicated by a green dashed rectangle with site labels $1-4$.

In this paper, we attempt to answer the following two questions: (1) What are the full phase diagram of the ferromagnetic and the antiferromagnetic Kitaev models in the presence of an external magnetic field pointing in arbitrary directions? (2) What are the essential effects of the additional Γ-Γ_p off-diagonal terms? Regarding the former, we identify a magnetization process with multiple topologically distinct phases depending on the field direction and strength. The phase boundaries are characterized by the first Chern number of the fermionic vacuum. Regarding the latter, we examine the phase diagram of the (K, Γ, Γ_p)-model and identified four different zero-field phases: a zigzag z (ZZ-z), a ferromagnetic (F), an extended KSL, and the Kitaev-Γ spin liquid (KΓSL) phase. A focus is given to the experimentally relevant ZZ-z phase, in which ferromagnetic chains are antiferromagnetically aligned perpendicular to the z bond. Our choice of the unit cell in Fig. 1 allows only for the ZZ-z phase. This discussion is elaborated further in Sec. IV B. Then, starting from the ZZ-z GS, we examine the magnetic field response as a function of the off-diagonal coupling strength Γ. We identify a region with reduced magnetization and decreased energy gap, named as the partially fractionalized (PF) phase. This phase is found to host strong partial spin fractionalization.

Throughout this paper, we employ a mean-field theory of the Majorana representation with local constraints. The advantage of this approach is that it readily captures the strong correlations inherent within this composite (fractionalized) representation along with the magnetic phases. We emphasize that the mean-field techniques should be considered as the pioneer strategy in the vast parameter space to guide more sophisticated yet expensive numerical techniques.

The article is divided into three sections. The current introductory section is completed with the discussion on the material aspects of the Kitaev model. In Sec. II, we present the mean-field theory scheme employed in this paper. Using this

approach, we then identify the topological Chern invariants for the pure AF/F Kitaev model for arbitrary magnetic-field orientations and strengths. The critical field strength and the angles for topological phase transitions are determined. In Sec. III, the role of the additional off-diagonal terms, Γ, Γ_p is examined. We complete this section by discussing the implications of our results for the recent thermal Hall experiments on candidate materials.

II. MATERIALS AND METHODS

A. A Kitaev material: α-RuCl$_3$

The experimental side of the search of Kitaev materials has advanced by signatures of massively degenerate, gapless excitations in the iridates X_2IrO_3 and in α-$RuCl_3$. The realistic modeling of these specific materials requires additional terms in the spin Hamiltonian. For concernant materials, the symmetry group is $\mathcal{D}_{3d} = \{\mathcal{I}, 2\mathcal{C}_3, 3\mathcal{C}_2, 2\mathcal{S}_6, 3\mathcal{M}\}$ [38,39,44,45], the symmetry allowed interactions can be cast into a general spin-spin coupling, $\Gamma_{ij}^{\alpha\beta} S_i^\alpha S_j^\beta$ where $\Gamma_{ij}^{\alpha\alpha} \to K, J$ and $\Gamma_{ij}^{\alpha\neq\beta} \to \Gamma, \Gamma_p$. The additional interactions and their role in the experimental findings are the subject of current experimental research [2,3,11–13,15–19], *ab initio* calculations [72], exact-diagonalization methods [73–75] and effective low-energy Hubbard Hamiltonians [32,76,77].

Here, we focus on α-$RuCl_3$ because there are several works in the literature to compare to and to ensure the validity of our approach in certain limits in $\Gamma - \Gamma_p$ space. $\alpha - RuCl_3$ crystals have a honeycomb structure of Ru-Ru bonds for a cut in the [111] direction (see Fig. 1). The Cl atoms are aligned as edge-sharing octahedra. The additional exchange paths through Ru-Cl bonds create a destructive interference for the otherwise leading term J, the Heisenberg exchange coupling [38,39]. Therefore, a Kitaev-type exchange coupling along with Γ and Γ_p terms takes stage. Experiments in zero magnetic field suggests a long range ZZ-z order for the GS of α-$RuCl_3$ [2,3,11–13,15–19]. Yet, a finite magnetic field melts the magnetic order and thereby allows for a transition to a spin liquid phase [14–17,57].

For the calculations described below, we switch to a new orthogonal coordinate system $(\hat{e}_1, \hat{e}_2, \hat{e}_3)$ with the following transformation:

$$\begin{pmatrix} \hat{e}_1 \\ \hat{e}_2 \\ \hat{e}_3 \end{pmatrix} = \frac{1}{\sqrt{6}} \begin{pmatrix} 1 & 1 & -2 \\ -\sqrt{3} & \sqrt{3} & 0 \\ \sqrt{2} & \sqrt{2} & \sqrt{2} \end{pmatrix} \begin{pmatrix} \hat{e}_x \\ \hat{e}_y \\ \hat{e}_z \end{pmatrix}. \tag{2}$$

Here, $\hat{e}_3$ points along the [111] direction, while the in-plane vectors $\hat{e}_1$ and $\hat{e}_2$ are perpendicular and parallel respectively to the z bonds.

B. A mean-field theory of Kitaev model

In materials like α-$RuCl_3$ and Na_2IrO_3, the Kitaev exchange coupling along all bond directions are likely to be equal [38,39]. We therefore consider an isotropic Kitaev coupling, $K^\alpha = K$. The isotropic model supports the trivial gapless B phase [1]. It can host two types of fractionalized excitations, the $\mathbb{Z}_2$ vortices and itinerant fermionic excitations, albeit a topologically trivial ground state. The system supports a topological phase in an external magnetic field along the [111] direction and thereby an energy gap opens proportional to $\Delta \sim \frac{h^3}{K^2}$ [1] where h is the magnetic field strength. The resulting phase is indexed by a finite integer Chern number. The concomitant neutral anyonic excitations lead to a quantized thermal Hall conductivity, i.e., they reveal themselves by a quantized response to a temperature gradient [1]. An intimate connection between the integer valued Chern number and the "half-integer" conductance arises [1].

In this section, we consider the Kitaev model in an arbitrarily oriented magnetic field within a mean-field theory scheme. We shall see that this approach reveals topological phase transitions as a function of the magnetic field strengths and orientations. The essential ingredients are described briefly below. An elaborated discussion of the mean-field approach is given in Appendix A where the authors discuss the detailed derivation, the role of quantum fluctuations as well as possible intrinsic bias. (Similar approaches have also been followed in Refs. [60–64,78–80].) The Hamiltonian takes the following form ($\mu_B = 1$):

$$H_K = \sum_{\langle ij \rangle}^{\alpha-bond} K^\alpha S_i^\alpha S_j^\alpha - \sum_{i,\beta} h^\beta S_i^\beta \tag{3}$$

where $\langle ij \rangle$ indicates nearest-neighbor sites on the honeycomb lattice and h^β is a component of the external magnetic field. As in [1], we replace the spin operators S_j^α by two composite Majorana operators b_j^α ($\alpha \in \{x, y, z\}$) and c_j as $S_j^\alpha = \frac{i}{2} b_j^\alpha c_j$ where $(b_j^\alpha)^2 = c_j^2 = 1$. This results in

$$H_K = \frac{K}{4} \sum_{\langle ij \rangle}^{\alpha-bond} i b_i^\alpha c_i i b_j^\alpha c_j - \frac{i}{2} \sum_{i,\beta} h^\beta b_i^\beta c_i. \tag{4}$$

The Kitaev Majorana representation doubles the Hilbert space size and the physical gauge sector is retained by the local gauge condition $D_j|\psi\rangle = |\psi\rangle$ where $D_j = b_j^x b_j^y b_j^z c_j$. We rewrite the local constraint $D_j = 1$ as $i\, b_j^\alpha c_j + i\frac{\epsilon^{\alpha\beta\gamma}}{2} b_j^\beta b_j^\gamma = 1$, where $\epsilon^{\alpha\beta\gamma}$ is the antisymmetric rank-3 tensor. The constraint is enforced by adding the term

$$H_\lambda = \frac{i}{2} \sum_j^\alpha \lambda_j^\alpha \left(b_j^\alpha c_j + \frac{\epsilon^{\alpha\beta\gamma}}{2} b_j^\beta b_j^\gamma \right), \tag{5}$$

with Lagrange multipliers, λ_j^α to the Hamiltonian, i.e., $H_K - H_\lambda$. The only terms that are not quadratic in Majorana variables in the Hamiltonian are the quartic terms in Eq. (4) arising from spin-spin interactions $S_i^\alpha S_j^\alpha$ in Eq. (3). We decompose these quartic terms into $\langle i b_i^\alpha c_i \rangle \times i b_j^\alpha c_j + \langle i b_i^\alpha b_j^\alpha \rangle \times -i c_i c_j + \ldots$ etc, resulting in an effective mean-field Hamiltonian, which is subsequently solved in a straightforward manner. The averages

$$m_A^\alpha = \langle i b_i^\alpha c_i \rangle, \quad m_B^\alpha = \langle i b_j^\alpha c_j \rangle, \tag{6}$$

$$w_\gamma = \langle -i c_i c_j \rangle_\gamma, \quad \Phi_\gamma^{\alpha\beta} = \langle i b_i^\alpha b_j^\beta \rangle_\gamma, \tag{7}$$

are treated as the mean-field parameters with respect to (w.r.t.) which the total energy E_{tot} will eventually be minimized. Here A, B are the honeycomb sublattice labels, and the subscripts γ indicate the bonds over which the averages are taken. We

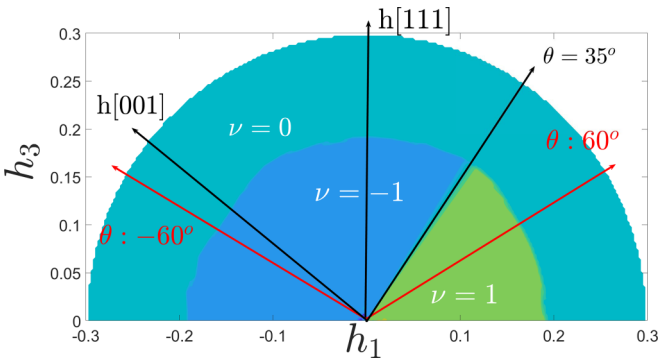

FIG. 2. Ferromagnetic Kitaev model: The Chern number map for arbitrary field direction and strength in the $(h_1 - h_3)$ plane, where $h_i = \mathbf{h} \cdot \hat{e}_i$ in units of $|K|$. Topologically distinct GSs with Chern numbers $\nu = \pm 1$ are identified. The trivial phase $\nu = 0$ corresponds to the high-field polarized phase. The red arrows indicate the experimental magnetic field angles that are used in Ref. [57] with $\theta = \pm 60^o$, where θ is the clockwise angle w.r.t. the h_3 axis. Note that $\theta = 35^o$ line corresponds to a direction in the $\hat{e}_x$ - $\hat{e}_y$ plane. The [001] direction is shown for visualization purposes.

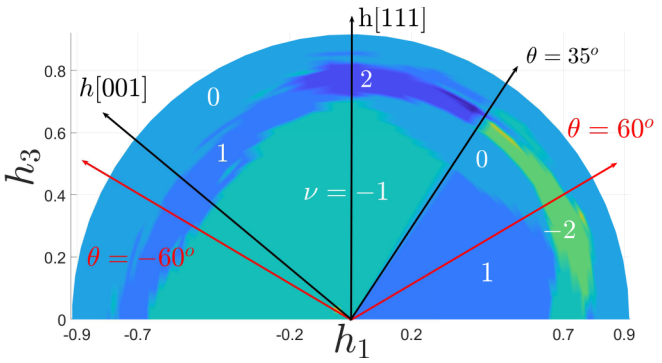

FIG. 3. Same as in Fig. 2 but the antiferromagnetic Kitaev model. There are in total five topologically distinct GSs possible with Chern numbers $\nu \in \{0, \pm 1, \pm 2\}$. The $\nu = 0$ phase is the field polarized phase. The red arrows indicate again the experimental magnetic field-angles that are used in Ref. [57].

demand $\frac{\partial E_{\text{tot}}}{\partial \lambda_i^\alpha} = 0$ from which a set of self-consistency equations follows.

Some comments are in order. If the averages corresponding to products of Majorana fermions on different sites, such as the bond operators $\Phi_\gamma^{\alpha\beta}$ are dropped or found to vanish, then the spins in the resulting state can be treated entirely as classical. On the other hand, if all averages on the same site such as m_i^α vanish, the result is analogous to Ref. [1], where the spins are completely fractionalized. In particular, for the pure Kitaev Hamiltonian in zero field, the absolute value of $\Phi_x^{xx} \equiv X$ attains its maximum possible value of 1, and similarly for $x \to y$ or z. We shall say in this case that the spins are "maximally fractionalized". In general, the values of X, Y, and Z thus describe the degree of fractionalization of the spins; they vanish in the classical limit. In this limit, the resulting effective Hamiltonian for the Majorana fermions is entirely local, and the Majorana bands have zero Chern numbers. In this respect, we emphasize that this mean-field method captures the quantum character of the model via the parameters X, Y, Z, and w_γ.

III. KITAEV MODEL IN AN ARBITRARY MAGNETIC FIELD

A. Ferromagnetic Kitaev model

We start with the ferromagnetic Kitaev model ($K < 0$), which has been extensively studied in the literature before [58,81]. We calculate the Chern number map in Fig. 2 for magnetic fields in the $a - c$ plane. The Chern numbers are calculated numerically following Ref. [82]. The radial axis in the selected directions mark the field strengths, $h = \sqrt{h_1^2 + h_2^2 + h_3^2}$ and $h_i = \mathbf{h} \cdot \hat{e}_i$. The upper half $(h_1 - h_3)$ plane is sufficient because reversing the field direction simply changes the sign of the Chern number [83].

In zero field, the KSL ground state is gapless. At small field strengths $0 < h \ll 1$, the fermionic vacuum becomes topologically nontrivial [1] with $\nu = \pm 1$ [84]. The odd valued Chern numbers indicate the presence of non-Abelian anyons [1] whereas even valued Chern numbers imply the presence of Abelian anyons. At higher fields beyond $h_c^F \approx 0.18|K|$, the system turns into a polarized, topologically trivial phase. The obtained sequence of states as a function of the magnetic field strength reproduces the previous result in Ref. [81]. In addition, there is an overall sign reversal (e.g., $\nu = 1 \to -1$) upon crossing the $\theta \approx 35^o$ line in the $h_1 - h_3$ plane [1,58]. Beware that the angle θ is defined w.r.t. the h_3 axis (clock-wise), e.g., positive angle means positive h_1 value. The sign change in ν can be naturally understood by a sign change of any magnetic field component (in this case h_z), because the Chern number is proportional to the sign of the energy gap created by the product of the magnetic field components, $\nu \sim \text{sgn}(h_x h_y h_z)$. Using the transpose of Eq. (2), the critical line (in the upper $h_1 - h_3$ plane) is identified by the angle where h_z changes sign, this is when $-\sqrt{2}h_1 + h_3 = 0$ or $\theta_c = \tan^{-1}(\frac{h_1}{h_3})\frac{180}{\pi} = 35^o$ is satisfied. The same sign changes apply to the antiferromagnetic Kitaev model as well.

Our approach captures all the qualitative properties of the field response for the F Kitaev model reported in the literature. On the quantitative side, the critical field strength for the transition to the polarized phase is found to be larger ($h_c^{\text{MF}} = 0.18|K|$) than the exact diagonalization results ($h_c^{ED} = 0.03\ |K|$) [58]. The latter result is more realistic because the current MF method neglects not only the additional correlations that cannot be described by a single particle wavefunctions but also the site dependent fluctuations of the constraint field (λ_i^α), which is strictly necessary to ensure a faithful representation of the spins as composite Majorana fermions. Hence, this drawback results in a larger window of stability for a spin liquid phase.

B. Antiferromagnetic Kitaev model

The antiferromagnetic Kitaev model is examined in two steps within the upper half of the $h_1 - h_3$ plane. The phase diagram is substantially different from $K < 0$ case. As noted before in [59,64], this can be understood as due to the difference in effective magnetic fields acting on the spins [59,64]. We first obtain the Chern number map as shown in Fig. 3.

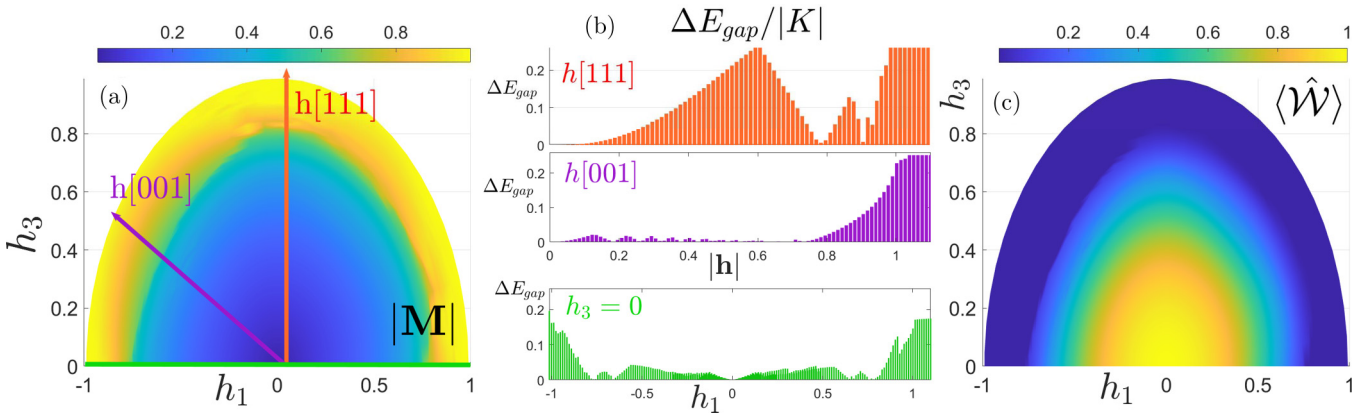

FIG. 4. Characterizing quantities of the antiferromagnetic Kitaev model: (a) The average magnetic moment, $|\mathbf{M}| = |\mathbf{m}_A + \mathbf{m}_B|/2$ within the upper $h_1 - h_3$ plane in units of $|K|$. The subscripts A and B are sublattice indices. The radial direction is the field strength. (b) The energy gap, ΔE_{gap} for cuts along the [111], [001], and $h_3 = 0$ directions as shown on plot a with red, purple and green lines respectively. (c) The MF contracted Wilson loop expectation value, $\langle\hat{\mathcal{W}}\rangle = 2^6\langle S_1^x S_2^y S_3^z S_4^x S_5^y S_6^z\rangle$ on a honeycomb plaquette. The maximum value, $\langle\hat{\mathcal{W}}\rangle = 1$ indicates a fractionalized KSL phase and thereby act as an order parameter.

We support this result by three additional results: The average magnetic moment $|\mathbf{M}| = |\mathbf{m}_A + \mathbf{m}_B|/2$ [Fig. 4(a)], the energy gap ΔE_{gap} [Fig. 4(b)] and the mean-field Wilson loop expectation value on a honeycomb plaquette, $\langle\hat{\mathcal{W}}\rangle = 2^6\langle S_1^x S_2^y S_3^z S_4^x S_5^y S_6^z\rangle$ [1] [Fig. 4(c)]. Note that the Wilson loop $\langle\hat{\mathcal{W}}\rangle$ allows to quantify the existence of an emergent gauge field, which is the direct signature of fractionalization where the spins fractionalize into local gauge fields (X, Y, and Z) and itinerant Majorana fermions (c_i). We calculate $\langle\hat{\mathcal{W}}\rangle$ by a MF contraction $\langle\hat{\mathcal{W}}\rangle \approx \langle ib_1^\alpha b_1^\alpha\rangle\langle -ic_i c_j\rangle + \ldots$, where the indices i, j stands for the sublattices A and B, respectively. For a two-site unit cell, the MF correlations for the six sites forming the honeycomb plaquette are not independent, but $\langle\hat{\mathcal{W}}\rangle \approx X^2Y^2Z^2$ where the c-type Majoranas have paired to unity, $c_i^2 = 1$ [85]. We omit all contractions, which reflect local magnetic moments, e.g., $\sim \langle ib_i^\alpha c_i\rangle$ to capture the gauge flux only.

We first consider the overall quantitative response of the AF Kitaev model, as shown in Fig. 4. The KSL phase stabilized in the $h \to 0$ limit crosses through an intermediate region with increasing field strengths and ultimately reaches a polarized phase. As shown in Fig. 4(a), $|\mathbf{M}|$ gradually increases and saturates at high-fields along all magnetic field directions. In parallel, the Wilson flux $\langle\hat{\mathcal{W}}\rangle$ [see Fig. 4(c)] decays with increasing field strength irrespective of the field orientation.

We first consider the evolution along the [111] ($\hat{e}_3$) direction, where $h_1 = h_2 = 0$. The role of the field direction is clearly visible in the topological index of the GS, the Chern number, ν in Fig. 3 (also see Appendix B and Fig. 8 for energy-band diagrams). The fermionic vacuum becomes topologically nontrivial ($\nu = -1$) and an energy gap opens proportional to $h_x h_y h_z/|K|^3$ [see the red-dashed curve on Fig. 4(b)]. At larger field strengths, there are two band touchings at $h \approx 0.7\ |K|$ and $0.8\ |K|$. Hence, four topologically distinct phases are encountered as a function of the field strength with the Chern numbers: $\nu = 0 \to -1 \to 2 \to 0$. At $h \approx 0.7\ |K|$, three additional Dirac cones are generated at the M points of the Brillouin zone, changing ν by 3 units $\nu = -1 \to 2$, with a noteworthy difference to Ref. [86] where the change is again in 3 units yet $\nu = -1 \to -4$ (w.r.t the Chern number sign convention of this paper). A scenario with a Chern number transfer of 3 is possible with an equal number of Dirac cones to be involved in this transition where each Dirac cone can transfer at most one unit of Chern number [87] via gap closure and reopening. The resulting even valued Chern number phase is supposed to have Abelian anyons [1]. In the high-field limit, eventually two Dirac cones annihilate each other (at gamma point) at $h \approx 0.8\ |K|$, resulting in ν from 2 to 0 with a polarized phase. The region with $\nu = 2$ is extended to the $h_1 \neq 0$ region as well as the corresponding finite energy gap in Fig. 4(b). The topological GS with a Chern number $\nu = 2$ has also been identified in Refs. [62,88] but both these references have confined themselves only to [111]. It has been asserted that this phase supports multiple Abelian anyonic species [88]. The conjectured "multispecies anyon" region extends mainly to positive θ angles as seen in Fig. 3. Along the negative θ direction, the $\nu = 2$ region is replaced by a phase with $\nu = 1$. These phases and others are also identified by the ΔE_{gap} map in Fig. 4(b).

The [001] field direction has already been investigated first in [60,81]. It was suggested that the ground state remains a gapless spin liquid until it reaches the field-polarized phase. The results of Nasu *et al.* [60] relied on a mean-field decoupling between "chains" of Wigner-Jordan strings, while Hickey and Trebst [81] employed numerical diagonalization of a small system. Similarly, we observe consecutive opening and closure of the energy gap in attenuating fashion until $h \approx 0.7\ |K|$ with the Chern number $\nu = 1$ [see the green curve on Fig. 4(b)]. Interestingly, ν does not change sign until $h \leqslant 0.7\ |K|$ and then it becomes $\nu = -1$ for $0.7 < h/|K| < 0.8$. At $h \approx 0.8\ |K|$, the system enters a trivial phase with a vanishing Chern number. In this respect, our MF approach provides a different field evolution along the [001] direction as compared to the literature.

An interesting transition occurs upon sweeping the magnetic field direction between the [001] and [111] directions (see Fig. 3) for two magnetic field strength limits. At high

field strengths, [001] and [111] directions are adiabatically connected with $\nu = 0$. Yet, at lower fields, the two directions are topologically distinct as [001] direction yields a gapless state [60,81]. We observe that the states in the vicinity of the [001] direction are topologically equivalent to the [111] direction with an energy gap and the same Chern number $\nu = -1$ in contrast to $\theta = 35^o$ where there is a topological transition. This transition was not noted before.

Before closing this section, we comment on the field directions $\theta = \pm 60^o$ and $\theta = \pm 90^o$ typically explored in experiments [57,58]. The experimentally accessible fields up to 50 Tesla allow α-$RuCl_3$ to cross all the phase boundaries. We therefore indicate the $\theta = \pm 60^o$ directions with red arrows in Figs. 2 and 3, whereas $\theta = \pm 90^o$ refers to the h_1 axis. It is clear that the field orientation dependence of κ_{xy} could be used to trace a AF type Kitaev term in real materials keeping in mind the material specific additional couplings. The change in κ_{xy} is expected to be in integer multiplies of $1/2$ in units of $\frac{\pi}{6}k_B^2 T$ [1]. Moreover, the topological transitions are accompanied by sign changes in κ_{xy} before the system reaches the high-field polarized phase.

IV. KITAEV-GAMMA (K-Γ-Γ_p) MODEL

A. Kitaev-gamma (K-Γ-Γ_p) model in zero field

In order to bridge the gap between experiments and theory, it is indispensable to include the additional terms readily present in candidate materials. The relevant terms are the off-diagonal exchange term is Γ, Γ_p as well as the Heisenberg coupling J. In the following, we consider less-frequently studied Γ and Γ_p terms [65–67,89–93], as they are sufficient to capture the ZZ-γ phase. The Hamiltonian for the additional terms is

$$H_{\Gamma,\Gamma_p} = \sum_{\langle ij\rangle,\beta\gamma}^{\alpha-bond} |\epsilon^{\alpha\beta\gamma}| \left[\Gamma S_i^\beta S_j^\gamma + \Gamma_p \left(S_i^\alpha S_j^\beta + S_i^\alpha S_j^\gamma\right)\right]. \quad (8)$$

The typical strengths of Γ and Γ_p are understood in various materials yet, there is no agreement [32] on precise values. For α-$RuCl_3$ [76], the magnitudes are estimated as $\Gamma \sim |K|$ and a small, negative Γ_p with $|\Gamma_p| \ll |K|$. For convenience, we partially relax the restriction on Γ, Γ_p to characterize the GS in a larger parameter space for positive Γ and negative Γ_p values.

Inspired by α-$RuCl_3$, we investigate the GS phase diagram for the K-Γ-Γ_p model again within the mean-field theory scheme. The decoupling of the quartic pieces in the Hamiltonian along with the off-diagonal spin-spin interactions now takes a more general form, $S_j^\alpha S_l^\beta$, i.e., on the γ bond, the spin-spin interaction and its mean-field decoupling read

$$\begin{aligned} -ib_i^\alpha b_j^\beta ic_i c_j \approx{}& \langle ib_i^\alpha c_i\rangle ib_j^\beta c_j + ib_i^\alpha c_i \langle ib_j^\beta c_j\rangle - \langle ib_i^\alpha c_i\rangle\langle ib_j^\beta c_j\rangle \\ &- \langle ib_i^\alpha b_j^\beta\rangle ic_i c_j + ib_i^\alpha b_j^\beta \langle -ic_i c_j\rangle \\ &- \langle b_i^\alpha b_j^\beta\rangle \langle -ic_i c_j\rangle \quad (9) \\ \equiv{}& m_A^\alpha ib_j^\beta c_j + m_B^\beta ib_i^\alpha c_i - m_A^\alpha m_B^\beta - \Phi_\gamma^{\alpha\beta} ic_i c_j + w_\gamma ib_i^\alpha b_j^\beta \\ &- \Phi_\gamma^{\alpha\beta} w_\gamma + \Delta_\gamma^\alpha ic_i b_j^\beta + \bar{\Delta}_\gamma^\beta ib_i^\alpha c_j - \Delta_\gamma^\alpha \bar{\Delta}_\gamma^\beta \quad (10) \end{aligned}$$

The additional MF parameters $\Phi_\gamma^{\alpha\beta} = \langle ib_i^\alpha b_j^\beta\rangle_\gamma$ as well as $\Delta_\gamma^\alpha = \langle ib_i^\alpha c_j\rangle_\gamma$ and $\bar{\Delta}_\gamma^\alpha = \langle ic_i b_j^\alpha\rangle_\gamma$ (see Appendix A) act as a way to destabilize the Kitaev spin liquid phase. Clearly, the bond operators $ib_i^\gamma b_j^\gamma$ on the γ bond, which commute with the pure Kitaev Hamiltonian are no longer constants of motion when Γ and Γ_p are nonzero.

The mean-field equations for the total Hamiltonian $H_{K\Gamma\Gamma_p} = H_K + H_{\Gamma\Gamma_p} - H_\lambda$ are solved for a four-site unit cell (see the green dashed rectangle in Fig. 1) so as to capture the relevant phases such as the ZZ-γ phase. In limiting to only four-site unit cells, we have also excluded states with larger unit cells [73] or incommensurate [39] order. At this point, it is underlined that we have limited our investigations to the ZZ phases to be ZZ-z only. It is known [44] that different zigzag phases can be favored under external fields, depending on the field directions. The energetic competition between these states is delicate and we prefer to leave that investigation to future work.

We fix the Kitaev coupling to be of ferromagnetic type ($K < 0$) and examine the phase diagram in Γ-Γ_p space in the zero field. Figures 5(a)–5(d) show the average magnetic moment ($|\mathbf{M}| = |\sum_{i=1}^4 \mathbf{m}_i|/4$ where the index i extends over the four-site unit cell), the staggered magnetic moment ($|\mathbf{M}_{\text{stag}}| = |\mathbf{m}_1 + \mathbf{m}_2 - \mathbf{m}_3 - \mathbf{m}_4|/4$), the Wilson flux and the energy gap (ΔE_{gap}), respectively. The parameters Γ and Γ_p cover of only the experimentally relevant ranges for α-$RuCl_3$ with $\Gamma \in [0, 0.62]$ and $\Gamma_p \in [-0.3, 0]$ in units of $|K|$. We identify four different phases, which are characterized below: KSL, KΓSL, F, and the ZZ-z phases. The F [73] and the ZZ-z phase are distinguished by the directions of the magnetic moments as well as by the vanishing Wilson flux [Fig. 5(c)] and the finite energy gap [Fig. 5(d)]. KSL and KΓSL phases have zero magnetic moments and gapless structure ($\Delta E_{\text{gap}} = 0$) and differ only in their average Wilson loop. Yet, the curve separating KSL phase and KΓSL phase should not be considered as a sharp boundary because the average Wilson flux is neither 1 or 0 but has a decaying form. The characteristic directions of the magnetic moments for each phase as summarized in Fig. 6(e).

Focusing on Fig. 5(a) first, there is an extended KSL region for small $|\Gamma_p|$ values. With increasing Γ values, there is a smooth crossover to a phase referred to as KΓSL [65,90]. It is also a gapless phase with zero Wilson flux average $\mathcal{W}$. For the region where $\Gamma < 0.3|K|$ and $\Gamma_p < -0.15|K|$, a ferromagnetic phase emerges. This phase can be understood by considering the spins as classical vectors for each sublattice, e.g., $\mathbf{S}_A^\alpha = \sin\theta_A \cos\phi_A \hat{x} + \sin\theta_A \sin\phi_A \hat{y} + \cos\theta_A \hat{z}$. Exploiting translational invariance, the energy (per unit cell) then reads

$$\begin{aligned} E ={}& 3(2\Gamma_p + \Gamma)\cos\theta_A \cos\theta_B + (K - (2\Gamma_p + \Gamma)) \\ &\times (\cos\theta_A \cos\theta_B \sin\theta_A \sin\theta_B \cos(\phi_A - \phi_B)). \quad (11) \end{aligned}$$

The minimization w.r.t. $\{(\theta_A, \phi_A), (\theta_B, \phi_B)\}$ implies all spins to align along the [111] direction.

Relevant to the candidate materials, there is a wide region in the Γ, Γ_p parameter plane with a ZZ-z phase as shown in Figs. 5(b) and 5(d). It is a gapped, topologically trivial and magnetically ordered phase [94]. The average magnetization $|\mathbf{M}|$ vanishes while the staggered magnetization is saturated

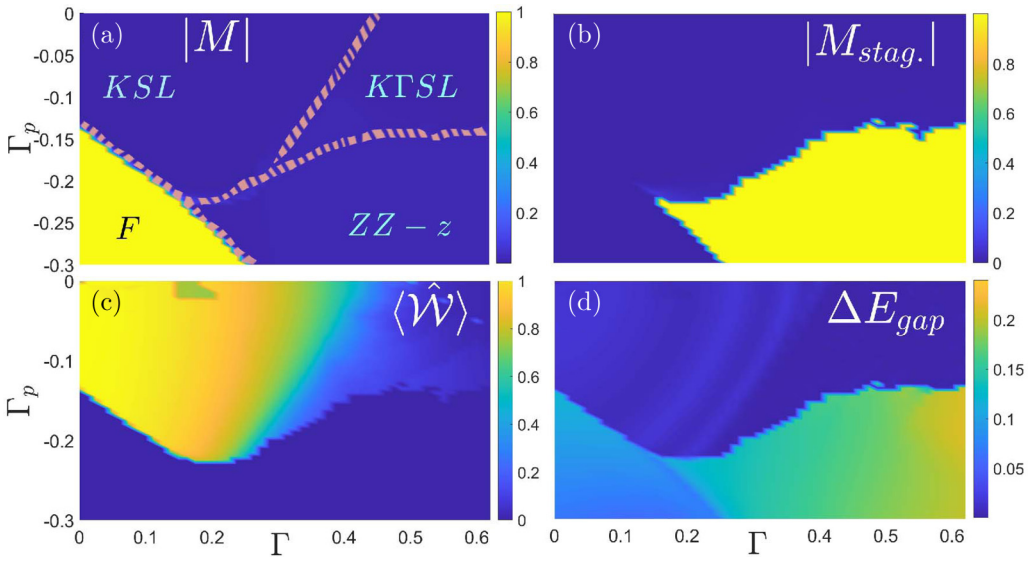

FIG. 5. The zero-field phase diagram of the K-Γ-Γ_p model for fixed ferromagnetic Kitaev term, $K < 0$. (a) Average total magnetization per four-site unit cell, $|\mathbf{M}| = |\sum_{i=1}^{4} \mathbf{m}_i|/4$. Two distinct regions are readily identified with either vanishing magnetization in the Kitaev spin liquid (KSL), the zigzag z phase (ZZ-z), the Kitaev-Γ spin liquid phase (KΓSL) and a saturated polarization in the ferromagnetic phase (F). All the phase boundaries are shown even if they cannot all be inferred from $|\mathbf{M}|$. (b) The staggered magnetization, $|\mathbf{M}_{stag.}| = |\mathbf{m}_1 + \mathbf{m}_2 - \mathbf{m}_3 - \mathbf{m}_4|/4$ reveals the ZZ-z phase. (c) The Wilson loop expectation value $\langle\hat{\mathcal{W}}\rangle$ in the mean-field factorization as a measure for the total strength of the emergent gauge field. A finite Wilson loop signals the fractionalization of spins into itinerant Majorana fermions as well as composite Majorana bond operators as gauge fields, and thereby distinguishes between the KSL and the KΓSL phase, i.e., $\langle\hat{\mathcal{W}}\rangle = 0$ in O and ZZ-z phase. (d) The energy gap is finite for the ZZ-z phase and the P phase and quantitatively different for each phase with zero Chern number. $\Delta E_{\text{gap}} = 0$ in the KSL and the KΓSL phase.

$|\mathbf{M}_{\text{stag}}| = 1$. For a four-site unit cell, the ZZ-z region is extended to larger Γ and Γ_p magnitudes. $|\mathbf{M}_{\text{stag}}|$ has thus the same value as one would find by assuming from the outset that the magnetic moments are purely classical instead of quantum mechanical. Though our method should be capable in capturing quantum mechanical spin fluctuations and hence a ZZ-z phase with $|\mathbf{M}_{\text{stag}}| < 1$ is in principle allowed, such a phase is not realized within the employed mean-field scheme.

B. Kitaev-gamma (K-Γ-Γ_p) model with magnetic field

In this section, we explore on the magnetic field response of the K-Γ-Γ_p model in $\Gamma - h$ space for the smallest value $\Gamma_p = -0.17|K|$, which stabilizes an experimentally relevant ZZ-z phase.

At zero field and with increasing Γ, there are four phases encountered: The P phase, the KSL phase, the KΓSL phase and the ZZ-z phase. We first orient the magnetic field along the experimentally often studied direction with $\theta = 60^o$ in the ac plane [57]. In Fig. 6, we present the phase diagram in which PF denotes a partially fractionalized phase. All the identified phases in $\Gamma - h$ space, shown in Fig. 6(a), are also illustrated with their local moment vectors in Fig. 6(e).

The P phase in which the magnetization points along the [111] ($\theta = 0^o$) direction for small Γ values was made evident already by the classical spin argument in Eq. (11). It is the phase labeled by (3) in Fig. 6(e). A finite field with $\theta = 60^o$ tilts the spins out of the [111] direction. A large enough field strength always takes the system into the P phase, although the critical strength depends on the value of Γ. Also, the direction of the spins lies between $\theta = 0^o$ and $\theta = 60^o$.

At larger Γ values for fixed $\Gamma_p = -0.17|K|$, the ferromagnetic phase is replaced by a KSL phase and it extends to larger field strengths. Because this region has a finite magnetization at any finite h, it can only be identified by a suppressed Wilson flux and a finite energy gap in Figs. 6(b) and 6(c), respectively. Depending on the strength of Γ, KSL can undergo a phase transition to either the P phase or the ZZ-z phase. There is a small area within the ZZ-z phase with a suppressed Wilson flux in the vicinity of the KSL region where the KΓSL phase seems to be stabilized. It is then replaced by the ZZ-z phase at much smaller field strengths.

Moreover, before the polarized phase, we indeed observe an intermediate phase with a reduced magnetic moment [see Fig. 6(a)], which we dubbed as the partially fractionalized (PF) phase. Even if it seems to be disconnected from the extended KSL region and has a vanishing Wilson flux [see Fig. 6(c)], this phase supports finite fractionalization. We plot the fractionalization order parameter $\sqrt{X^2 + Y^2 + Z^2}$, e.g., $X = \langle ib_j^x b_l^x \rangle_x$, [see Fig. 6(f)] showing that the total spin fractionalization is finite within the PF phase (see Fig. 9 for additional indicators along $\theta = -60^o$). It is a gapped phase [see Fig. 6(d)] and exists for a wide range of Γ values.

The antisymmetrized thermal Hall conductivity $\kappa_{xy}^A = (\kappa_{xy} - \kappa_{yx})/2$ is routinely measured in the THC experiments (see e.g., [57–59]). Near zero temperature, the linear T coefficient of κ_{xy}^A is proportional to the total Chern number ν of the occupied fermionic bands. Hence, we now discuss ν obtained in our mean-field theory for the K-Γ-Γ_p model in

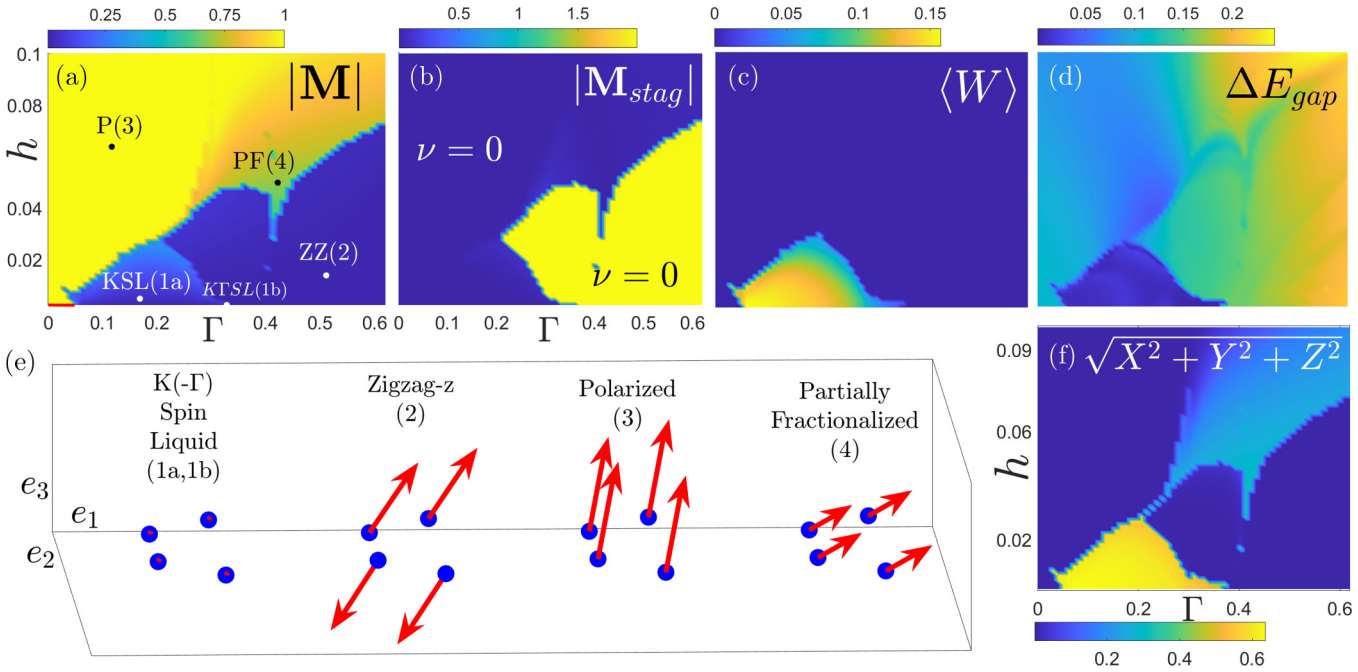

FIG. 6. K-Γ-Γ_p model in a tilted magnetic field for $\theta = 60^o$ w.r.t. c axis for $K < 0$ and $\Gamma_p = -0.17|K|$ in Γ-h space. (a) The total magnetization per four-site unit cell, $|\mathbf{M}| = |\sum_{i=1}^{4} \mathbf{m}_i|/4$. (b) The staggered magnetization per four-site unit cell, $|\mathbf{M}_{\text{stag}}| = (|\mathbf{m}_1 + \mathbf{m}_2 - \mathbf{m}_3 - \mathbf{m}_4|/4)$. The staggered definition is used to distinguish the ZZ-z phase. Using plots (a) and (b), one can identify four different phases: KSL, ZZ-z, PF (partially fractionalized or intermediate), and P phases. Note that, the ZZ-z phase and the P phase regions have trivial topology, $\nu = 0$. (c) The Wilson flux expectation per plaquette. The finite region denoted with yellow-orange colors indicates the KSL states, whereas the remaining regions is either highly suppressed with the absence of fractionalization or negative values indicating another polarized phase. (d) The energy gap for the ground state. It reveals a detailed information on how to distinguish each phase. The energy gap vanishes for the KSL while partially suppressed for the intermediate PF phase. (e) The magnetic moment vectors for the four-site unit cell. The points with their numbers are indicated on plot (a). (f) The total spin fractionalization order parameter for the bond-correlations, $\sqrt{X^2+Y^2+Z^2}$ where say X is defined as $\langle ib_j^x b_l^x \rangle_x$. This plot makes evident that the PF phase hosts fractionalized bond correlations for larger magnitudes of the magnetic field.

a magnetic field. Firstly, at $h = 0$ in Fig. 5, the ZZ-z phase is a collinear phase, which can be mapped back to itself by a time-reversal operator and a translation by a lattice vector. Naturally, it indicates a trivial Chern number. Within the PF phase, the system is connected with the P phase at high magnetic fields without a gap closure, it has $\nu = 0$ in spite of finite spin fractionalization. The linear T coefficient of κ_{xy}^A is thus expected to vanish, but a contribution from thermal excitations across the relatively small gap is possible. Also, for the P phase at large magnetic fields, the spins are polarized and the correlations between the Majorana fermions are completely local, giving only topologically trivial bands and hence also $\nu = 0$. We have numerically verified $\nu = 0$ for the ZZ-z phase and the P phase.

We now extend the analysis of the K-Γ-Γ_p model to arbitrary field directions. The absolute magnetization in arbitrary magnetic field (in the a-c plane) is shown in Fig. 7, where $M_{abs} = \frac{1}{4}\sum_{i=1}^{4} |\mathbf{m}_i|$. We set the couplings as $K < 0, \Gamma = 0.5|K|$, $\Gamma_p = -0.17|K|$ such that the GS is the ZZ-z phase. The radial direction is the magnetic field strength and θ is the polar angle w.r.t. the c axis. The ZZ-z phase is stable for small field strengths in all directions. The field extended ZZ-z phase is also seen in other studies [44,73], if Γ is comparable to the Kitaev coupling. It is known [44] that the ZZ-z phase is more stable to out-of-plane magnetic field, since the spins can tilt more easily towards the field direction. For $\Gamma < |K|$, $\mathbf{M}_{\text{stag}}$ tends to a more acute angle with the $x-y$ plane ($\theta = 35^o$), with a small out-of-plane z component. In the presence of a magnetic field pointing closer to the z direction ($\theta = -55^o$), the ZZ-z phase is hence more stable in comparison to the field directions within the x-y plane ($\theta = 35^o$). In this regard, the THC experiment on α-$RuCl_3$ has revealed that the magnetic field responses for $\theta = \pm 60^o$ directions are not symmetrical but the system has a wider intermediate region for $\theta = +60^o$ [58]. We indeed verify a wider intermediate region (less stable ZZ-z phase) for $\theta = 60^o$ compared to -60^o. On the contrary, for the field directions closer to the x-y plane (θ is around 35° or -150^o), the ZZ-z phase is highly unstable and paves the way for the intermediate PF phase. Because the magnetic field is not along [111], the rotational symmetry is already broken and we therefore cannot address the nematic phases reported in literature [73].

V. CONCLUSIONS

We developed a Majorana mean-field theory for complicated Kitaev materials. It holds a good basis for the investigation of expensive Hamiltonians to hunt for spin liquids to complement time and resource consuming numerical approaches within large parameter spaces. One such model that a MF Majorana theory is applied [95] is the

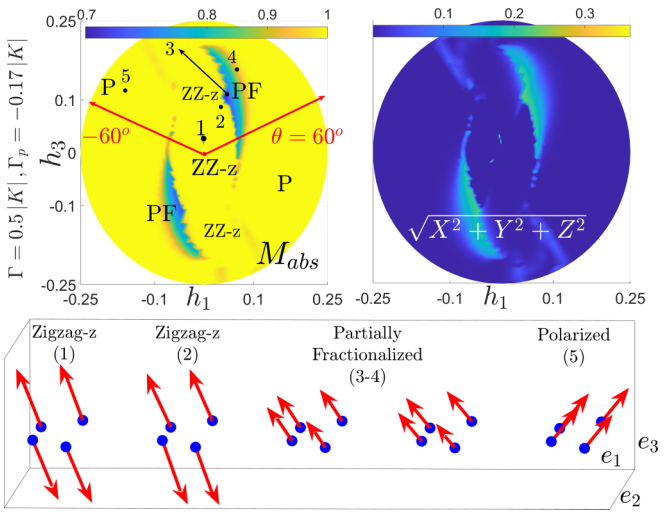

FIG. 7. (a) The absolute magnetization per site in $h_1 - h_3$ space: $M_{abs} = \frac{1}{4}\sum_{i=1}^{4} |\mathbf{m}_i|$. The model parameters are chosen to host a ZZ-z GS for $K < 0$, $\Gamma = 0.5|K|$ and $\Gamma_p = -0.17|K|$ in zero field. Four different phases are identified: The zero-field ZZ-z (1) phase extends up to a critical field strength extending to point (2) with a wider range along the $h_1 = 0$ line. The partially fractionalized PF (3) phase is stable within a confined region extending to point (4) at intermediate field strengths. Finally, the P phase (5) takes over at high field strengths. The corresponding magnetic moment vectors of each site in a four-site unit cell are labeled from 1 to 5 in the lower panel. The orientations of the vectors follow the field directions. (b) The total spin fractionalization for the bond correlations, $\sqrt{X^2+Y^2+Z^2}$, highlighting the fractionalization in the PF phase.

two-dimensional J_1-J_2 Heisenberg model, which could have applicability to cuprates.

We sum up this work by referring back to the initially posed questions. Regarding the phase diagram of the AF Kitaev model in a magnetic field: We identified an additional topologically nontrivial ground state with Abelian anyons (even Chern number $\nu = \pm 2$) in addition to the $\nu = \pm 1$ vacuum mainly referred to in the literature as the source of the half-quantized THC. The magnetic field response is sensitive to the magnetic field orientation and strength upon, which several topological transitions are encountered for fields in the a-c plane. We emphasize that the gapless phases are hard to trace and demand for special numerical care (e.g., for fields in the [001] direction).

Regarding the role of the additional off-diagonal Γ-Γ_p terms in the modeling of real materials, we have shown that the pure Kitaev picture changes dramatically for comparable strength of $\Gamma \sim |K|$ in favor of a KΓSL as the gauge-flux expectation value per plaquette vanishes, $\mathcal{W} = 0$. At finite Γ_p and not too small Γ, the zigzag phase emerges. At a finite magnetic field, the KΓSL phase gave way to the zigzag phase. Starting from these phases at zero field, a magnetic field of suitable strength is able to drive the system towards partial spin fractionalization. The latter phase however is different from the Kitaev spin liquid as indicated by the Wilson flux. Further investigation of the properties of this phase with partial fractionalization region is left to the future.

Comparing our results with the theoretical results readily available in the literature, we not only found a qualitatively satisfying agreement for all limits of K, Γ, Γ_p, and $\mathbf{h}$ but we made two important contributions, the topologically distinct sectors of the pure AF Kitaev model in different magnetic field orientations and the coexistence of magnetic moments and fractionalization dubbed as the PF phase for K-Γ-Γ_p-$\mathbf{h}$ model. Additionally, our findings also capture the asymmetry in the magnetic field response measurements in Ref. [58] for $\theta = \pm 60^o$ magnetic field orientations in a straightforward way.

It is worth talking about typical magnetic field strengths and the relevance of the numbers obtained in this paper to experiments. In Fig. 6, the magnetic field direction along $\theta = 60^o$, the PF phase is stabilized mainly for $h \in [0.05, 0.12]$ (in units of $|K|$). Matching the energy scales for the Kitaev

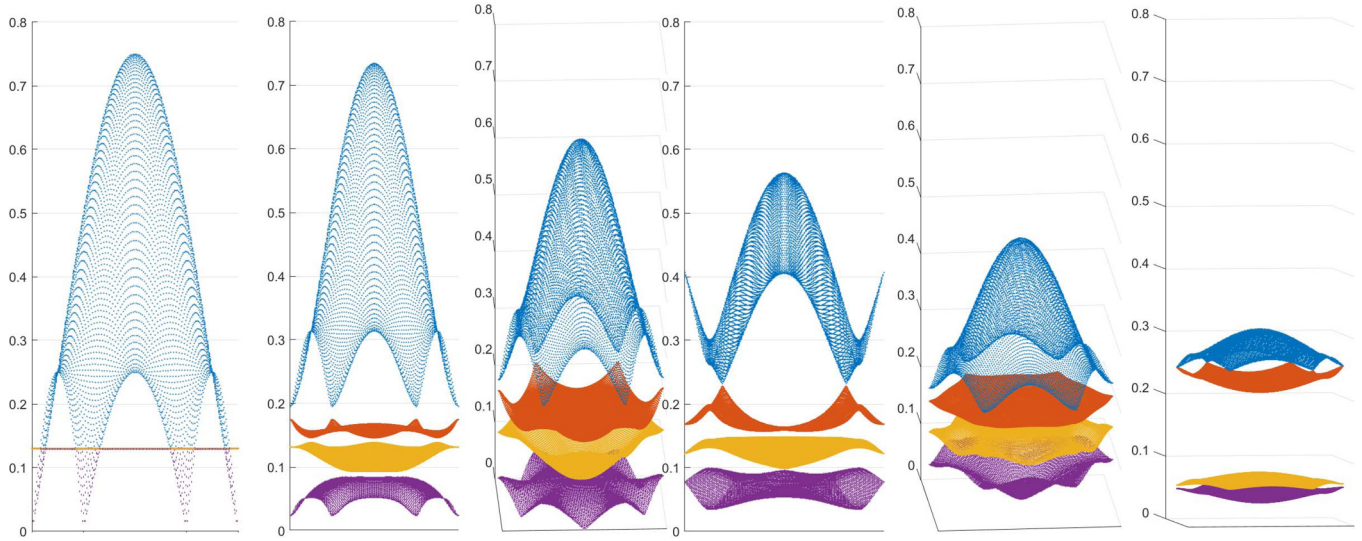

FIG. 8. The energy band diagram for the AF Kitaev model under [111] magnetic field. Leftmost plot is $h = 0$ KSL limit whereas the rightmost plot is the polarized limit ($h = K$). There are two critical field strengths at $h_c = 0.7K, 0.8K$ where Dirac cones occur and leading to a topological transition.

coupling and the magnetic field coupling term, $\vec{h}\cdot\vec{S} = K$, one can get a rough estimate on the magnetic field scale. $0.05k_B|K| \leqslant Bg_J\mu_B j_{\text{eff}} \leqslant 0.12|K|$ yields a window for the magnetic field strength $B \in [4, 9.4]$ T. Note that Kitaev coupling is estimated to be roughly $100K$ [96]. Also, $j_{\text{eff}} = S = 1/2$, k_B is the Boltzmann constant, μ_B is the Bohr magneton and $g_J \approx 2$ is the Lande factor for j_{eff}. In Fig. 7, the width of PF phase is varying as a function of magnetic field direction. The critical field for melting the ZZ-z phase can go up to 16+ Tesla for [111] direction and even larger for small and negative θ values. These findings are verified with the literature [96] (and references therein such as Ref. [97]) and show that the Majorana MF theory predicts sensible results.

This paper raises several questions to be addressed in a next step as a natural extension, in particular about the character of the intermediate phase. A detailed study of the nature of the excitations of this partially fractionalized phase could provide valuable information relevant for spectroscopic signatures. Aside from the current materials of interest, there is an extended region [98] with $\Gamma > 0$ and $\Gamma_p > 0$ in spin liquid phases are stabilized. Actually, preliminary results premise an even larger extended region of stabilized KSL phase for $\Gamma < 0$ and $\Gamma_p > 0$. Even an additional region stabilizing a ZZ-z phase in $\Gamma - \Gamma_p$ space is possible, which could potentially provide an alternative materials scenario. A finite temperature response of the $K - \Gamma - \Gamma_p$ model in arbitrary magnetic field is indispensable for conclusions with regards to thermal Hall conductivity experiments. Thermodynamical functions need to be calculated for a wide regime of $K - \Gamma - \Gamma_p - h - T$ parameters. Additionally, we aim at analytical evaluations for the thermodynamics of the antiferromagnetic Kitaev model in a [001] magnetic field with closed form expressions in leading orders of h and T. And it has to be explored how our conceptually simple and comprehensive formalism can be applied to comply with the recently observed oscillations [59] in the longitudinal thermal conductivity as a function of the inverse magnetic field.

ACKNOWLEDGMENTS

A.P.K. was supported by the Deutsche Forschungsgemeinschaft (DFG, German Research Foundation) through Project No. 107745057 TRR 80. Part of this work was performed while FSY was in Taiwan, S.K.Y. and F.Y. were supported by the Ministry of Science and Technology, Taiwan, under Grant No. MOST 107-2112-M-001-035-MY3 and No. MOST 108-2811-M-001-618, respectively.

APPENDIX A: KITAEV SPIN LIQUID (KSL): MEAN-FIELD APPROXIMATION

Before we start, let us define our convention for the symbols used in the Appendix: ρ, θ, η are used for x, y, z type Pauli matrix indices (unlike the main manuscript where we used α, β, γ). α, β, γ symbols are instead used to distinguish Majorana fermions and take the values $\{\pm4, \pm3, \pm2, \pm1\}$. Negative values are for sublattice A and positive values are reserved for sublattice B, respectively. Finally, the symbol λ is used for two different purposes: A Lagrange multiplier or a subscript index in the diagonal reciprocal space basis.

For the Kitaev model in Eq. (1), a solution attempt by Jordan-Wigner slave fermions leads to a quartic interaction term on the z bonds [60,99]. However, this approach is not very useful for arbitrary field directions where one has to deal with Pauli strings [60]. We therefore stick to Kitaev's original representation [1]. Accordingly, each spin is represented by two Majorana fermions—as real fermionic field. Consider the following mapping (with $\hbar = 1$):

$$2S_j^\rho = \sigma_j^\rho = ib_j^\rho c_j, \quad \rho \in \{x, y, z\}, \tag{A1}$$

$$\left\{b_i^\rho, b_j^\theta\right\} = 2\delta_{\rho,\theta}\delta_{i,j}, \quad \left\{b_i^\rho, c_j\right\} = 0, \tag{A2}$$

$$\left(b_i^\rho\right)^2 = c_i^2 = 1. \tag{A3}$$

Each spin component is thus a composite object consisting of two Majorana fermions. However, the size of the Hilbert space is thereby doubled and it is required to impose the following quartic constraint at each site to ensure the equivalence and the reality of each vector in the enlarged Hilbert space,

$$\hat{D}_j = b_j^x b_j^y b_j^z c_j = 1. \tag{A4}$$

In the new representation the Kitaev Hamiltonian is written as

$$H_K = \frac{1}{4}\sum_{jl,\rho-bond} K^\rho b_j^\rho b_l^\rho c_j c_l. \tag{A5}$$

The spectral decomposition of H_K is obtained by using the constants of motion, the bond operators $\hat{u}_{jl}^\rho \equiv ib_j^\rho b_l^\rho$, $[H_K, \hat{u}_{jl}^\rho] = 0$. In other words, each bond gauge field is a constant of motion and the Hilbert space can be segmented into the gauge sectors of each bond. Choosing all gauge-sector eigenvalues as $\hat{u}_{jl}^\rho = +1$ for $K^\rho > 0$, the gauge fields are "frozen" and decoupled from itinerant fermions. Then, the Hamiltonian becomes quadratic,

$$H_K = -\frac{i}{4}\sum_{jl,\rho-bond} K^\rho c_j c_l. \tag{A6}$$

The itinerant fermion dispersion [1] is

$$\epsilon(\mathbf{q}) = \pm|K^x e^{i\mathbf{q}\cdot\mathbf{r}_x} + K^y e^{i\mathbf{q}\cdot\mathbf{r}_y} + K^z e^{i\mathbf{q}\cdot\mathbf{r}_z}|, \tag{A7}$$

which is identical to the graphene with Dirac cones when $K^\alpha = K$. The bond vectors [in $\hat{e}_1, \hat{e}_2, \hat{e}_3$ basis as shown in Eq. (2)] are $\mathbf{r}_x = -2(2\mathbf{a}_1 - \mathbf{a}_2)/3$, $\mathbf{r}_y = -2(2\mathbf{a}_2 - \mathbf{a}_1)/3$ and $\mathbf{r}_z = (2\mathbf{a}_1 + \mathbf{a}_2)/3$. The Bravais vectors of the honeycomb lattice are $\mathbf{a}_1 = \frac{\sqrt{3}a}{2}(1, \sqrt{3})$ and $\mathbf{a}_2 = \frac{\sqrt{3}a}{2}(-1, \sqrt{3})$ with a being the lattice constant. However, this approach is highly sensitive to proper gauge choices in each sector, therefore it is very limited for extensions to other interactions, which are readily present in real materials. Moreover, the additional emerging exchange couplings demand a more all-inclusive approach in which fractional and conventional magnetism can be treated on an equal footing. A mean-field decoupling of Majorana fermions [60–64,78–80] in this respect is a suitable method for two reasons: Firstly, a decoupling scheme provides the desired competition between the conventional and the anomalous pairings. Secondly, the main disadvantage of a typical mean-field (MF) method, i.e., the loss of correlations, is partially resolved because the fractionalized excitations are

already included through replacing the spin operators by composite Majorana operators.

Kitaev type spin-spin interaction has a quartic form in Majorana representation. The bond operators $\hat{u}^{\alpha}_{jl}$ are not frozen in a more general setting, e.g., in the presence of the external field, additional off-diagonal spin-spin interactions. It is therefore more appropriate to decouple a general spin-spin interaction on an arbitrary bond η, e.g., $S^{\rho}_j S^{\theta}_l$ as follows:

$$\begin{aligned} -ib^{\rho}_j b^{\theta}_l ic_j c_l \approx & \langle ib^{\rho}_j c_j\rangle ib^{\theta}_l c_l + ib^{\rho}_j c_j \langle ib^{\theta}_l c_l\rangle - \langle ib^{\rho}_j c_j\rangle\langle ib^{\theta}_l c_l\rangle \\ & - \langle ib^{\rho}_j b^{\theta}_l\rangle ic_j c_l + ib^{\rho}_j b^{\theta}_l\langle - ic_j c_l\rangle \\ & - \langle b^{\rho}_j b^{\theta}_l\rangle\langle - ic_j c_l\rangle \\ \equiv & \, m^{\rho}_A ib^{\theta}_l c_l + m^{\rho}_B ib^{\theta}_j c_j - m^{\rho}_A m^{\theta}_B - \Phi^{\rho\theta}_{\eta} ic_j c_l \\ & + w_{\eta} ib^{\rho}_j b^{\theta}_l - \Phi^{\rho\theta}_{\eta} w_{\eta}. \end{aligned} \tag{A8}$$

Assuming isotropic bond strengths, $K^{\alpha} = K$, the MF decoupled magnetic Kitaev mean-field Hamiltonian reads

$$\begin{aligned} H_K = & \frac{K}{4} \sum_{jl,\rho-bond} \left(m^{\rho}_A - \frac{2h^{\rho}}{K}\right) ib^{\alpha}_l c_l + \left(m^{\rho}_B - \frac{2h^{\rho}}{K}\right) ib^{\rho}_j c_j \\ & - \Phi^{\rho\rho}_{\rho} ic_j c_l + w^{\rho} ib^{\rho}_j b^{\rho}_l - m^{\rho}_A m^{\rho}_B - \Phi^{\rho\rho}_{\rho} w_{\rho}. \end{aligned} \tag{A9}$$

Corresponding MF parameters are

$$m^{\rho}_A = \langle ib^{\rho}_j c_j\rangle, \quad m^{\rho}_B = \langle ib^{\rho}_l c_l\rangle, \tag{A10}$$

$$w_{\rho} = -\langle ic_j c_l\rangle_{\rho}, \quad \Phi^{\rho\theta}_{\eta} = \langle ib^{\rho}_j b^{\theta}_l\rangle_{\eta}. \tag{A11}$$

Note that $m^{\rho}_{A,B}$ are components of the local magnetic moments on sublattices A and B whereas $w_{\eta} = w$ is the same on all bonds. $\Phi^{\rho\theta}_{\eta}$ are the indicators of fractionalization defined on the bond η. For simplicity, we use shorthand notations for $\Phi^{\eta\eta}_{\eta}$, e.g., $\Phi^{xx}_{x} = X$. While the aim is to obtain a quadratic Hamiltonian, there is an issue regarding the quartic constraint on Majorana fermions. The strategy is to rewrite the constraint in terms of two-fermion operators. Multiplying both sides with any two of the four fermion operators, one can rewrite the single quartic constraint in Eq. (A4) as three quadratic constraint relations,

$$b^z c + b^x b^y = 0, \tag{A12}$$

$$b^x c + b^y b^z = 0, \tag{A13}$$

$$b^y c + b^z b^x = 0, \tag{A14}$$

where the site index is dropped for simplicity. Based on these relations, the constraints can be introduced into the Hamiltonian with three Lagrange multipliers,

$$H_{\rm MF} = H_K - H_{\lambda}, \;\; H_{\lambda} = \frac{i}{2} \sum_{j}^{\rho,\theta,\eta\in\{x,y,z\}} \lambda^{\rho} \left(b^{\rho}_j c_j + \frac{\epsilon^{\rho\theta\eta}}{2} b^{\theta}_j b^{\eta}_j\right), \tag{A15}$$

where we omitted any spatial dependence of $\lambda^{\rho}_i = \lambda^{\rho}$. The constrained mean-field Hamiltonian must satisfy the saddle point condition

$$\frac{\partial\langle H_{\rm MF}\rangle}{\partial\lambda^{\rho}} = \frac{\partial E_{\rm tot}(\lambda)}{\partial\lambda^{\rho}} = 0, \tag{A16}$$

which is equivalent to the quadratic constraints to hold for expectation values,

$$\langle ib^z c\rangle = -\langle ib^x b^y\rangle, \tag{A17}$$

$$\langle ib^x c\rangle = -\langle ib^y b^z\rangle, \tag{A18}$$

$$\langle ib^y c\rangle = -\langle ib^z b^x\rangle. \tag{A19}$$

For the evaluation of $\langle H_{\rm MF}\rangle$ we consider the general Hamiltonian (H) of the form

$$H = -i \sum_{j\alpha,l\beta} \epsilon_{j\alpha,l\beta} c_{j\alpha} c_{l\beta} \tag{A20}$$

on a periodic lattice. Here $c_{j\alpha}$ operators, unlike c_j, includes all types of Majorana fermions (b^x, b^y, b^z, c). j, l labels are unit cells indices for sublattices A and B, respectively. The sub-indices α, β represent the Majorana flavors (e.g., $c_{j,\{-4,-3,-2,-1\}} \in \{b^x_j, b^y_j, b^z_j, c_j\}$ and $c_{j,\{1,2,3,4\}} \in \{b^x_l, b^y_l, b^z_l, c_l\}$) within the corresponding sublattices. $\epsilon_{j\alpha,l\beta}$ is necessarily anti-symmetric under the interchange $j\alpha \leftrightarrow l\beta$. This Hamiltonian can be diagonalized using the transformation

$$c_{j\alpha} = \sqrt{2} \sum_{\mathbf{q},\lambda} u_{j\alpha,\mathbf{q},\lambda} \alpha_{\mathbf{q},\lambda} \tag{A21}$$

where $\sqrt{2}$ is used to ensure the correct factor in the anticommutation relations. The coefficients $u_{j\alpha,\mathbf{q},\lambda}$ satisfy the eigenvalue equation,

$$E_{\mathbf{q},\lambda} u_{j\alpha,\mathbf{q},\lambda} = -i\epsilon_{j\alpha,l\beta} u_{l\beta,\mathbf{q},\lambda}. \tag{A22}$$

$\mathbf{q}$ labels the wavevector and $\lambda \in \{\pm4, \pm3, \pm2, \pm1\}$ labels eight different solutions at each $\mathbf{q}$. The eigenvectors imply a plane-wave form

$$u_{j\alpha,\mathbf{q},\lambda} = \frac{1}{\sqrt{N}} e^{i\mathbf{q}\cdot\mathbf{r}_j} \tilde{u}_{\alpha\lambda}(\mathbf{q}). \tag{A23}$$

Here, N is the number of unit cells, $\mathbf{r}_j$ is the position vector of the sublattice A site j, and $\mathbf{r}_j = j_1\mathbf{a}_1 + j_2\mathbf{a}_2$. For convenience we choose $\sum_{\alpha} |\tilde{u}_{\alpha\lambda}(\mathbf{q})|^2 = 1$. Equations (A20) and (A21) imply that the operators $\alpha_{\mathbf{q},\lambda}$ satisfy the commutation relation

$$[\alpha_{\mathbf{q},\lambda}, H] = E_{\mathbf{q},\lambda} \alpha_{\mathbf{q},\lambda}. \tag{A24}$$

Explicitly, $\alpha_{\mathbf{q},\lambda} = \frac{1}{\sqrt{2}} \sum_{j,\alpha} u^*_{j\alpha,\mathbf{q},\lambda} c_{j\alpha}$ can be derived from Eq. (A20). Equation (A21) transforms H into

$$H = \frac{1}{2} \sum_{\mathbf{q},\lambda} E_{\mathbf{q},\lambda} \alpha^{\dagger}_{\mathbf{q},\lambda} \alpha_{\mathbf{q},\lambda}. \tag{A25}$$

Taking the complex conjugate of Eq. (A22) tells that the eigenvalues come in pairs: If $u_{l\alpha,\mathbf{q},\lambda}$ is a solution with eigenenergy $E_{\mathbf{q},\lambda}$, then $u_{l\alpha,-\mathbf{q},-\lambda} = u^*_{l\alpha,\mathbf{q},\lambda}$ (belonging to wavevector $-\mathbf{q}$) has eigenenergy $-E_{\mathbf{q},\lambda}$, and the associated operator $\alpha_{-\mathbf{q},-\lambda}$ is equivalent to $\alpha^{\dagger}_{\mathbf{q},\lambda}$. Rewriting the diagonalized Hamiltonian in Eq. (A25) in terms of positive energy oper-

ators only, we obtain

$$H = \frac{1}{2}\sum_{\mathbf{q},\lambda}^{E_{\mathbf{q},\lambda}>0}[E_{\mathbf{q},\lambda}\alpha^{\dagger}_{\mathbf{q},\lambda}\alpha_{\mathbf{q},\lambda} - E_{\mathbf{q},\lambda}\alpha_{\mathbf{q},\lambda}\alpha^{\dagger}_{\mathbf{q},\lambda}]$$
$$= \sum_{\mathbf{q},\lambda}^{E_{\mathbf{q},\lambda}>0} E_{\mathbf{q},\lambda}\alpha^{\dagger}_{\mathbf{q},\lambda}\alpha_{\mathbf{q},\lambda} - \frac{1}{2}\sum_{\mathbf{q},\lambda}^{E_{\mathbf{q},\lambda}>0} E_{\mathbf{q},\lambda} \tag{A26}$$

where the sums extend over only the positive energy eigenstates. $\alpha_{\mathbf{q},\lambda}$ operators satisfy the usual anticommutation relations $\{\alpha_{\mathbf{q},\lambda_1}, \alpha^{\dagger}_{\mathbf{q}',\lambda_2}\} = \delta_{\mathbf{q},\mathbf{q}'}\delta_{\lambda_1,\lambda_2}$. The ground state, therefore, is defined as $\alpha_{\mathbf{q},1}|GS\rangle = 0$. This representation is useful for finite temperature extensions.

Specifically for this paper, $\epsilon_{j\alpha,l\beta}$ corresponds to the mean-field parameters in Eq. (A10) and Eq. (A11) entering the mean-field Hamiltonian H_{MF} in Eq. (A9). The Hamiltonian has an 8×8 matrix representation $\mathcal{H}_{\mathbf{q}}$ in momentum space. Our convention is

$$H_{\mathrm{MF}} = \sum_{\mathbf{q}} \Psi^{\dagger}_{\mathbf{q}}\mathcal{H}_{\mathbf{q}}\Psi_{\mathbf{q}}, \tag{A27}$$

where $\Psi_{\mathbf{q}} = (b^x_{\mathbf{q}}, b^y_{\mathbf{q}}, b^z_{\mathbf{q}}, c_{\mathbf{q}}, \bar{b}^x_{\mathbf{q}}, \bar{b}^y_{\mathbf{q}}, \bar{b}^z_{\mathbf{q}}, \bar{c}_{\mathbf{q}})$ indicates the Fourier transformed Majorana operators. The momentum space operators with(out) a bar on top belong to the sublattice-B (A), e.g., $b^{\alpha}_{l} \leftrightarrow \bar{b}^{\alpha}_{\mathbf{q}}$ ($b^{\alpha}_{j} \leftrightarrow b^{\alpha}_{\mathbf{q}}$). Yet, we generalize this convention to $c_{\mathbf{q}\alpha}$ operators where each operator in $\Psi_{\mathbf{q}}$ is represented by α index, where $\alpha \in \{\pm 4, \pm 3, \pm 2, \pm 1\}$. $\mathcal{H}_{\mathbf{q}}$ can be diagonalized as $\Gamma^{\dagger}_{\mathbf{q}}\mathcal{H}_{\mathbf{q}}\Gamma_{\mathbf{q}} = D_{\mathbf{q}}$ where the matrix $\Gamma_{\mathbf{q}}$ has the form

$$\Gamma_{\mathbf{q}} = (|\mathbf{q}, -4\rangle ... |\mathbf{q}, -1\rangle |\mathbf{q}, 1\rangle ... |\mathbf{q}, 4\rangle). \tag{A28}$$

$|\mathbf{q}, \lambda\rangle = \alpha^{\dagger}_{\mathbf{q},\lambda}|0\rangle$ denotes 8-component vectors where $u_{j\alpha,\mathbf{q}\lambda} = \langle j\alpha|\mathbf{q}, \lambda\rangle$. Thereby the matrix elements of $\Gamma_{\mathbf{q}}$ are $\tilde{u}_{\alpha\lambda}(\mathbf{q})$ in Eq. (A23) with α, λ being the entries for rows and columns, respectively.

The mean-field analysis is concluded by the self-consistency relations for the MF parameters. For bond correlations, self-consistency requires

$$\langle ic_{j\alpha}c_{l\beta}\rangle = \frac{2i}{N}\sum_{\mathbf{q},\lambda}^{E_{\mathbf{q},\lambda}>0} e^{i\mathbf{q}\cdot\mathbf{r}_{\gamma}}\tilde{u}_{\alpha\lambda}(\mathbf{q})\tilde{u}^{*}_{\beta\lambda}(\mathbf{q}), \tag{A29}$$

where the site indices j, l determine the bond direction $\mathbf{r}_{\gamma} = \mathbf{r}_j - \mathbf{r}_l$. The self-consistency cycle is completed via the dependence of $\tilde{u}_{\alpha\lambda}(\mathbf{q})$ on the MF parameters.

The values of α, β, γ for each MF parameters are provided below. Regarding the bond correlations,

$$X \to \alpha = -4, \beta = 1, \gamma = x,$$
$$Y \to \alpha = -3, \beta = 2, \gamma = y,$$
$$Z \to \alpha = -2, \beta = 3, \gamma = z,$$
$$w^{\gamma} \to \alpha = -1, \beta = 4, \gamma \in \{x, y, z\} \quad \text{with a "–" sign}$$

Regarding the local correlations (e.g., magnetic moments),

$$\langle ic_{j\alpha}c_{j\beta}\rangle = \frac{2i}{N}\sum_{\mathbf{q},\lambda}^{E_{\mathbf{q},\lambda}>0} \tilde{u}_{\alpha\lambda}(\mathbf{q})\tilde{u}^{*}_{\beta\lambda}(\mathbf{q}). \tag{A30}$$

The parameters are defined as

$$m^x_A \to \alpha = -4, \beta = -1, \quad m^x_B \to \alpha = 1, \beta = 4,$$
$$m^y_A \to \alpha = -3, \beta = -1, \quad m^y_B \to \alpha = 2, \beta = 4,$$
$$m^z_A \to \alpha = -2, \beta = -1, \quad m^z_B \to \alpha = 3, \beta = 4.$$

The remaining MF parameters [e.g., in Eq. (A17)] can be handled with a similar straightforward approach.

We used a two-site unit cell for pure Kitaev models under a magnetic field whereas a four-site unit cell for K-Γ-Γ_p model in a crystal. The Bravais lattice vectors for a two-site unit cell, $\mathbf{a}_1, \mathbf{a}_2$ are shown below Eq. (A7) and the four-site unit-cell vectors $\tilde{\mathbf{a}}_1, \tilde{\mathbf{a}}_2$ are chosen as $\tilde{\mathbf{a}}_1 = \mathbf{a}_1 - \mathbf{a}_2$ and $\tilde{\mathbf{a}}_2 = \mathbf{a}_1 + \mathbf{a}_2$. Regarding the four-site unit cell, it can be argued if the BZ backfolding in a reduced BZ poses a problem for a ground state with a two-site periodicity due to the redundant energy level crossings at the BZ boundary. Yet, it is a well-known fact that the energy level crossings in the reciprocal space does not have a topological origin and the energy eigenstates are equivalent compared to the case where there is no back-folding in a two-site unit cell. The Brillouin zone integrals are approximated as 10000+ meshpoint sums for the Brillouin zone, $\int_{BZ} d^2k \approx \sum_i (\Delta k)_i$. The Chern number for a two-site unit cell is calculated [82] for a simpler rhombic Brillouin zone choice. It is because the Wilson loops at the boundaries of the BZ could pose problems due to the complicated periodicity of the honeycomb shaped BZ. Moreover, one has the freedom to choose any set of unique $\mathbf{q}$ points in the reciprocal space as the basis vectors. The initial configurations for the MF parameters as well as the Lagrange multipliers are set to various distinct values such that the minimization procedure can capture all possible phases, e.g., P, ZZ-z, PF and spin liquid phases. The ground state is the lowest energy configuration satisfying convergence conditions w.r.t the MF parameters and their total mean squared error threshold in the gradient descent scheme. The threshold is 10^{-6} for stable regions, 10^{-4} for the phase boundaries with stronger variations in MF parameters. We also checked the performance of the mean-field method in magnetic fields. Neither the magnetic field strength nor the magnetic field angle changes the performance of the mean-field method.

APPENDIX B: THE ENERGY-BAND EVOLUTION ALONG [111] DIRECTION

Here, we provide the energy band evolution for the AF Kitaev model under a magnetic field along [111] direction. An infinitesimal field strength gaps the system with a Chern number $\nu = -1$. At an intermediate field strength, $h = 0.7K$, there are three Dirac cones occur at M-points of the Brillouin zone as well as a Chern number transfer by 3 unit, where the ground state Chern number is $\nu = 2$. Then, two Dirac cones merge and annihilate at Gamma point at larger field strengths with a topologically trivial P phase.

APPENDIX C: THE DETAILS OF THE K-Γ-Γ_p MODEL IN A MAGNETIC FIELD

In Fig. 9, we plot the bond correlations (X, Y and Z) and the itinerant Majorana correlations (w^{α}) for the K-Γ-Γ_p

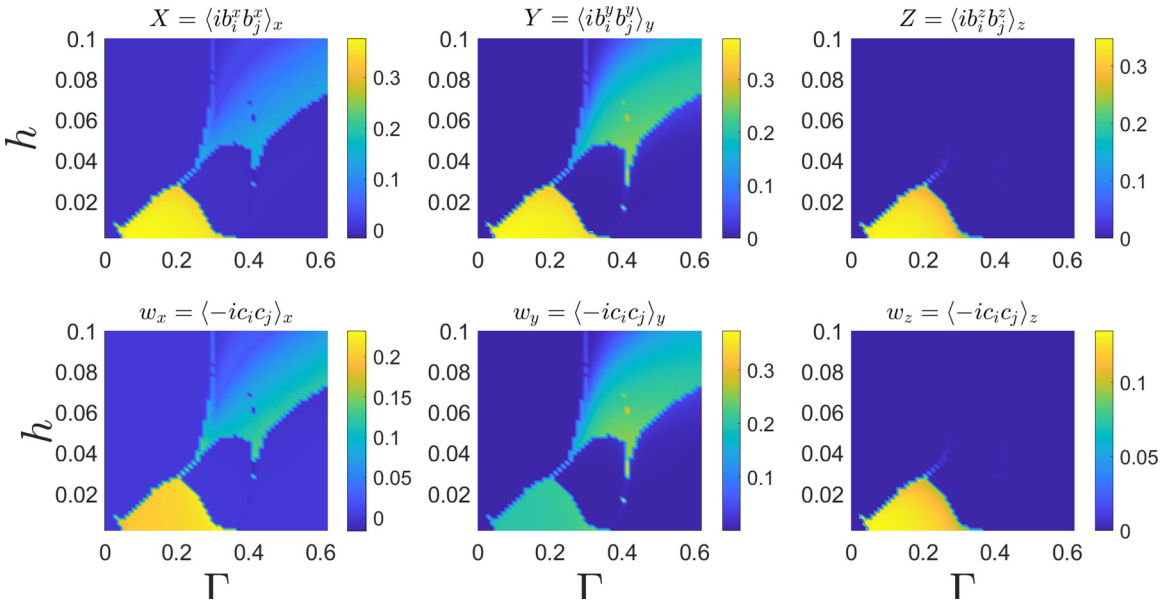

FIG. 9. The spin fractionalization order parameters for the K-Γ-Γ_p model, averaged over the four site unit cell, as function of field strength h and the off-diagonal spin interaction strength Γ. Field direction is along $\theta = -60^o$. The bond-correlations X, Y, and Z (e.g., $X = \langle ib_j^x b_l^x \rangle_x$) are given in the first row whereas the itinerant Majorana correlations w^α, $w^x = \langle ic_j c_l \rangle_x$ are shown in the second row. A nonzero value indicates spin fractionalization.

model in a $\theta = -60^o$ magnetic field in $\Gamma - h$ space with fixed $\Gamma_p = -0.17|K|$. The extended KSL regime is visible as a hill-shaped region at the bottom left corner of each plot. In the intermediate PF regime, the residual fractionalization is visible along the supported by the finite bond correlations for X, Y as well as w_x and w_y throughout the PF regime. Because the field direction is close to [001] direction, the hybridization between b^z and c Majorana fermions strongly suppresses the fractionalization along the z bonds.

[1] A. Kitaev, Anyons in an exactly solved model and beyond, Ann. Phys. **321**, 2 (2006).

[2] S. Williams, R. Johnson, F. Freund, S. Choi, A. Jesche, I. Kimchi, S. Manni, A. Bombardi, P. Manuel, P. Gegenwart, and R. Coldea, Incommensurate counterrotating magnetic order stabilized by Kitaev interactions in the layered honeycomb α-Li_2IrO_3, Phys. Rev. B **93**, 195158 (2016).

[3] M. Majumder, R. Manna, G. Simutis, J. Orain, T. Dey, F. Freund, A. Jesche, R. Khasanov, P. Biswas, E. Bykova, N. Dubrovinskaia, L. S. Dubrovinsky, R. Yadav, L. Hozoi, S. Nishimoto, A. A. Tsirlin, and P. Gegenwart, Breakdown of Magnetic Order in the Pressurized Kitaev Iridate β-Li_2IrO_3, Phys. Rev. Lett. **120**, 237202 (2018).

[4] S. Choi, R. Coldea, A. Kolmogorov, T. Lancaster, I. Mazin, S. Blundell, P. Radaelli, Y. Singh, P. Gegenwart, K. Choi, S.-W. Cheong, P. J. Baker, C. Stock, and J. Taylor, Spin Waves and Revised Crystal Structure of Honeycomb Iridate Na_2IrO_3, Phys. Rev. Lett. **108**, 127204 (2012).

[5] F. Ye, S. Chi, H. Cao, B. C. Chakoumakos, J. A. Fernandez-Baca, R. Custelcean, T. Qi, O. Korneta, and G. Cao, Direct evidence of a zigzag spin-chain structure in the honeycomb lattice: A neutron and X-ray diffraction investigation of single-crystal Na_2IrO_3, Phys. Rev. B **85**, 180403 (2012).

[6] Y. Singh, S. Manni, J. Reuther, T. Berlijn, R. Thomale, W. Ku, S. Trebst, and P. Gegenwart, Relevance of the Heisenberg-Kitaev Model for the Honeycomb Lattice Iridates A_2IrO_3, Phys. Rev. Lett. **108**, 127203 (2012).

[7] H. Gretarsson, J. Clancy, Y. Singh, P. Gegenwart, J. Hill, J. Kim, M. Upton, A. Said, D. Casa, T. Gog, and Y.-J. Kim, Magnetic excitation spectrum of Na_2IrO_3 probed with resonant inelastic x-ray scattering, Phys. Rev. B **87**, 220407 (2013).

[8] Y. Yamaji, Y. Nomura, M. Kurita, R. Arita, and M. Imada, First-Principles Study of the Honeycomb-Lattice Iridates Na_2IrO_3 in the Presence of Strong Spin-Orbit Interaction and Electron Correlations, Phys. Rev. Lett. **113**, 107201 (2014).

[9] Z. Alpichshev, F. Mahmood, G. Cao, and N. Gedik, Confinement-Deconfinement Transition as an Indication of Spin-Liquid-Type Behavior in Na_2IrO_3, Phys. Rev. Lett. **114**, 017203 (2015).

[10] D. Wulferding, Y. Choi, S.-H. Do, C. H. Lee, P. Lemmens, C. Faugeras, Y. Gallais, and K.-Y. Choi, Magnon bound states versus anyonic Majorana excitations in the Kitaev honeycomb magnet α-$RuCl_3$, Nat. Commun. **11**, 1603 (2020).

[11] Y. Kubota, H. Tanaka, T. Ono, Y. Narumi, and K. Kindo, Successive magnetic phase transitions in α-$RuCl_3$: XY-like frustrated magnet on the honeycomb lattice, Phys. Rev. B **91**, 094422 (2015).

[12] P. Lampen-Kelley, S. Rachel, J. Reuther, J.-Q. Yan, A. Banerjee, C. A. Bridges, H. B. Cao, S. E. Nagler, and D. Mandrus, Anisotropic susceptibilities in the honeycomb Kitaev system α-$RuCl_3$, Phys. Rev. B **98**, 100403 (2018).

[13] K. Plumb, J. Clancy, L. Sandilands, V. V. Shankar, Y. Hu, K. Burch, H.-Y. Kee, and Y.-J. Kim, α-$RuCl_3$: A spin-orbit assisted

Mott insulator on a honeycomb lattice, Phys. Rev. B **90**, 041112 (2014).

[14] I. A. Leahy, C. A. Pocs, P. E. Siegfried, D. Graf, S.-H. Do, K.-Y. Choi, B. Normand, and M. Lee, Anomalous Thermal Conductivity and Magnetic Torque Response in the Honeycomb Magnet α-$RuCl_3$, Phys. Rev. Lett. **118**, 187203 (2017).

[15] S.-H. Baek, S.-H. Do, K.-Y. Choi, Y. S. Kwon, A. Wolter, S. Nishimoto, J. van den Brink, and B. Büchner, Evidence for a Field-Induced Quantum Spin Liquid in α-$RuCl_3$, Phys. Rev. Lett. **119**, 037201 (2017).

[16] Z. Wang, S. Reschke, D. Hüvonen, S.-H. Do, K.-Y. Choi, M. Gensch, U. Nagel, T. Rõõm, and A. Loidl, Magnetic Excitations and Continuum of a Possibly Field-Induced Quantum Spin Liquid in α-$RuCl_3$, Phys. Rev. Lett. **119**, 227202 (2017).

[17] J. Zheng, K. Ran, T. Li, J. Wang, P. Wang, B. Liu, Z.-X. Liu, B. Normand, J. Wen, and W. Yu, Gapless Spin Excitations in the Field-Induced Quantum Spin Liquid Phase of α-$RuCl_3$, Phys. Rev. Lett. **119**, 227208 (2017).

[18] C. Balz, L. Janssen, P. Lampen-Kelley, A. Banerjee, Y. H. Liu, J.-Q. Yan, D. G. Mandrus, M. Vojta, and S. E. Nagler, Field-induced intermediate ordered phase and anisotropic interlayer interactions in α-$RuCl_3$, Phys. Rev. B **103**, 174417 (2021).

[19] A. Banerjee, P. Lampen-Kelley, J. Knolle, C. Balz, A. A. Aczel, B. Winn, Y. Liu, D. Pajerowski, J. Yan, C. A. Bridges *et al.*, Excitations in the field-induced quantum spin liquid state of α-$RuCl_3$, npj Quantum Mater. **3**, 8 (2018).

[20] L. J. Sandilands, Y. Tian, K. W. Plumb, Y.-J. Kim, and K. S. Burch, Scattering Continuum and Possible Fractionalized Excitations in α-$RuCl_3$, Phys. Rev. Lett. **114**, 147201 (2015).

[21] L. J. Sandilands, Y. Tian, A. A. Reijnders, H.-S. Kim, K. W. Plumb, Y.-J. Kim, H.-Y. Kee, and K. S. Burch, Spin-orbit excitations and electronic structure of the putative Kitaev magnet α-$RuCl_3$, Phys. Rev. B **93**, 075144 (2016).

[22] M. Majumder, M. Schmidt, H. Rosner, A. Tsirlin, H. Yasuoka, and M. Baenitz, Anisotropic Ru^{3+} $4d^5$ magnetism in the α-$RuCl_3$ honeycomb system: Susceptibility, specific heat, and zero-field NMR, Phys. Rev. B **91**, 180401 (2015).

[23] S. Bachus, D. Kaib, Y. Tokiwa, A. Jesche, V. Tsurkan, A. Loidl, S. Winter, A. A. Tsirlin, R. Valentí, and P. Gegenwart, Thermodynamic Perspective on Field-Induced Behavior of α-$RuCl_3$, Phys. Rev. Lett. **125**, 097203 (2020).

[24] S. Reschke, V. Tsurkan, S.-H. Do, K.-Y. Choi, P. Lunkenheimer, Z. Wang, and A. Loidl, Terahertz excitations in α-$RuCl_3$: Majorana fermions and rigid-plane shear and compression modes, Phys. Rev. B **100**, 100403 (2019).

[25] X.-G. Zhou, H. Li, Y. H. Matsuda, A. Matsuo, W. Li, N. Kurita, K. Kindo, and H. Tanaka, Intermediate quantum spin liquid phase in the Kitaev material α-$RuCl_3$ under high magnetic fields up to 100 T, arXiv:2201.04597

[26] H. Liu and G. Khaliullin, Pseudospin exchange interactions in d^7 cobalt compounds: Possible realization of the Kitaev model, Phys. Rev. B **97**, 014407 (2018).

[27] H. Liu, J. Chaloupka, and G. Khaliullin, Kitaev Spin Liquid in 3D Transition Metal Compounds, Phys. Rev. Lett. **125**, 047201 (2020).

[28] G. Lin, J. Jeong, C. Kim, Y. Wang, Q. Huang, T. Masuda, S. Asai, S. Itoh, G. Günther, M. Russina *et al.*, Field-induced quantum spin disordered state in spin-1/2 honeycomb magnet $Na_2Co_2TeO_6$, Nat. Commun. **12**, 5559 (2021).

[29] C. Kim, J. Jeong, G. Lin, P. Park, T. Masuda, S. Asai, S. Itoh, H.-S. Kim, H. Zhou, J. Ma *et al.*, Antiferromagnetic Kitaev interaction in $j_{\rm eff} = 1/2$ cobalt honeycomb materials $Na_3Co_2SbO_6$ and $Na_2Co_2TeO_6$, J. Phys.: Condens. Matter **34**, 045802 (2022).

[30] S.-H. Jang, R. Sano, Y. Kato, and Y. Motome, Antiferromagnetic Kitaev interaction in f-electron based honeycomb magnets, Phys. Rev. B **99**, 241106 (2019).

[31] Y. Motome and J. Nasu, Hunting Majorana fermions in Kitaev magnets, J. Phys. Soc. Jpn. **89**, 012002 (2020).

[32] S. M. Winter, A. A. Tsirlin, M. Daghofer, J. van den Brink, Y. Singh, P. Gegenwart, and R. Valenti, Models and materials for generalized Kitaev magnetism, J. Phys.: Condens. Matter **29**, 493002 (2017).

[33] L. Balents, Spin liquids in frustrated magnets, Nature (London) **464**, 199 (2010).

[34] L. Savary and L. Balents, Quantum spin liquids: A review, Rep. Prog. Phys. **80**, 016502 (2017).

[35] Y. Zhou, K. Kanoda, and T.-K. Ng, Quantum spin liquid states, Rev. Mod. Phys. **89**, 025003 (2017).

[36] C. Broholm, R. Cava, S. Kivelson, D. Nocera, M. Norman, and T. Senthil, Quantum spin liquids, Science **367**, eaay0668 (2020).

[37] J. Knolle and R. Moessner, A field guide to spin liquids, Annu. Rev. Condens. Matter Phys. **10**, 451 (2019).

[38] G. Jackeli and G. Khaliullin, Mott Insulators in the Strong Spin-Orbit Coupling Limit: From Heisenberg to a Quantum Compass and Kitaev Models, Phys. Rev. Lett. **102**, 017205 (2009).

[39] J. G. Rau, E. K.-H. Lee, and H.-Y. Kee, Generic Spin Model for the Honeycomb Iridates beyond the Kitaev Limit, Phys. Rev. Lett. **112**, 077204 (2014).

[40] F.-Y. Li, Y.-D. Li, Y. Yu, A. Paramekanti, and G. Chen, Kitaev materials beyond iridates: Order by quantum disorder and Weyl magnons in rare-earth double perovskites, Phys. Rev. B **95**, 085132 (2017).

[41] Y. Motome, R. Sano, S. Jang, Y. Sugita, and Y. Kato, Materials design of Kitaev spin liquids beyond the Jackeli-Khaliullin mechanism, J. Phys.: Condens. Matter **32**, 404001 (2020).

[42] U. Kumar, S. Banerjee, and S.-Z. Lin, Floquet engineering of kitaev quantum magnets, Commun. Phys. **5**, 157 (2022).

[43] S. Chaudhary, A. Ron, D. Hsieh, and G. Refael, Controlling ligand-mediated exchange interactions in periodically driven magnetic materials, arXiv:2009.00813.

[44] L. Janssen, E. C. Andrade, and M. Vojta, Magnetization processes of zigzag states on the honeycomb lattice: Identifying spin models for α-$RuCl_3$ and Na_2IrO_3, Phys. Rev. B **96**, 064430 (2017).

[45] V. M. Katukuri, S. Nishimoto, V. Yushankhai, A. Stoyanova, H. Kandpal, S. Choi, R. Coldea, I. Rousochatzakis, L. Hozoi, and J. van den Brink, Kitaev interactions between $j = 1/2$ moments in honeycomb Na_2IrO_3 are large and ferromagnetic insights from ab initio quantum chemistry calculations, New J. Phys. **16**, 013056 (2014).

[46] P. Laurell and S. Okamoto, Dynamical and thermal magnetic properties of the Kitaev spin liquid candidate α-$RuCl_3$, npj Quantum Mater. **5**, 2 (2020).

[47] H.-S. Kim, A. Catuneanu, H.-Y. Kee *et al.*, Kitaev magnetism in honeycomb $RuCl_3$ with intermediate spin-orbit coupling, Phys. Rev. B **91**, 241110 (2015).

[48] L. Wu, A. Little, E. E. Aldape, D. Rees, E. Thewalt, P. Lampen-Kelley, A. Banerjee, C. A. Bridges, J.-Q. Yan, D. Boone, S. Patankar, D. Goldhaber-Gordon, D. Mandrus, S. E. Nagler, E. Altman, and J. Orenstein, Field evolution of magnons in α-$RuCl_3$ by high-resolution polarized terahertz spectroscopy, Phys. Rev. B **98**, 094425 (2018).

[49] O. Tanaka, Y. Mizukami, R. Harasawa, K. Hashimoto, K. Hwang, N. Kurita, H. Tanaka, S. Fujimoto, Y. Matsuda, E.-G. Moon *et al.*, Thermodynamic evidence for a field-angle-dependent Majorana gap in a Kitaev spin liquid, Nat. Phys. **18**, 429 (2022).

[50] J. Cookmeyer and J. E. Moore, Spin-wave analysis of the low-temperature thermal Hall effect in the candidate Kitaev spin liquid α-$RuCl_3$, Phys. Rev. B **98**, 060412 (2018).

[51] P. McClarty, X.-Y. Dong, M. Gohlke, J. Rau, F. Pollmann, R. Moessner, and K. Penc, Topological magnons in Kitaev magnets at high fields, Phys. Rev. B **98**, 060404 (2018).

[52] M. Ye, R. M. Fernandes, and N. B. Perkins, Phonon dynamics in the Kitaev spin liquid, Phys. Rev. Res. **2**, 033180 (2020).

[53] É. Lefrançois, G. Grissonnanche, J. Baglo, P. Lampen-Kelley, J.-Q. Yan, C. Balz, D. G. Mandrus, S. E. Nagler, S. Kim, Y.-J. Kim, N. Doiron-Leyraud, and L. Taillefer, Evidence of a Phonon Hall Effect in the Kitaev Spin Liquid Candidate α-$RuCl_3$, Phys. Rev. X **12**, 021025 (2022).

[54] Y. H. Gao, C. Hickey, T. Xiang, S. Trebst, and G. Chen, Thermal Hall signatures of non-Kitaev spin liquids in honeycomb Kitaev materials, Phys. Rev. Res. **1**, 013014 (2019).

[55] Y. Kasahara, K. Sugii, T. Ohnishi, M. Shimozawa, M. Yamashita, N. Kurita, H. Tanaka, J. Nasu, Y. Motome, T. Shibauchi, and Y. Matsuda, Unusual Thermal Hall effect in a Kitaev Spin Liquid Candidate α-$RuCl_3$, Phys. Rev. Lett. **120**, 217205 (2018).

[56] R. Hentrich, M. Roslova, A. Isaeva, T. Doert, W. Brenig, B. Büchner, and C. Hess, Large thermal Hall effect in α-$RuCl_3$: Evidence for heat transport by Kitaev-Heisenberg paramagnons, Phys. Rev. B **99**, 085136 (2019).

[57] Y. Kasahara, T. Ohnishi, Y. Mizukami, O. Tanaka, S. Ma, K. Sugii, N. Kurita, H. Tanaka, J. Nasu, Y. Motome *et al.*, Majorana quantization and half-integer thermal quantum Hall effect in a Kitaev spin liquid, Nature (London) **559**, 227 (2018).

[58] T. Yokoi, S. Ma, Y. Kasahara, S. Kasahara, T. Shibauchi, N. Kurita, H. Tanaka, J. Nasu, Y. Motome, C. Hickey *et al.*, Half-integer quantized anomalous thermal Hall effect in the Kitaev material candidate α-$RuCl_3$, Science **373**, 568 (2021).

[59] P. Czajka, T. Gao, M. Hirschberger, P. Lampen-Kelley, A. Banerjee, J. Yan, D. G. Mandrus, S. E. Nagler, and N. Ong, Oscillations of the thermal conductivity in the spin-liquid state of α-$RuCl_3$, Nat. Phys. **17**, 915 (2021).

[60] J. Nasu, Y. Kato, Y. Kamiya, and Y. Motome, Successive Majorana topological transitions driven by a magnetic field in the Kitaev model, Phys. Rev. B **98**, 060416 (2018).

[61] L. Janssen and M. Vojta, Heisenberg-Kitaev physics in magnetic fields, J. Phys.: Condens. Matter **31**, 423002 (2019).

[62] A. Ralko and J. Merino, Novel Chiral Quantum Spin Liquids in Kitaev Magnets, Phys. Rev. Lett. **124**, 217203 (2020).

[63] S. Liang, M.-H. Jiang, W. Chen, J.-X. Li, and Q.-H. Wang, Intermediate gapless phase and topological phase transition of the Kitaev model in a uniform magnetic field, Phys. Rev. B **98**, 054433 (2018).

[64] K. Ido and T. Misawa, Correlation effects on the magnetization process of the Kitaev model, Phys. Rev. B **101**, 045121 (2020).

[65] J. S. Gordon, A. Catuneanu, E. S. Sørensen, and H.-Y. Kee, Theory of the field-revealed Kitaev spin liquid, Nat. Commun. **10**, 2470 (2019).

[66] A. Catuneanu, Y. Yamaji, G. Wachtel, Y. B. Kim, and H.-Y. Kee, Path to stable quantum spin liquids in spin-orbit coupled correlated materials, npj Quantum Mater. **3**, 23 (2018).

[67] Z.-X. Liu and B. Normand, Dirac and Chiral Quantum Spin Liquids on the Honeycomb Lattice in a Magnetic Field, Phys. Rev. Lett. **120**, 187201 (2018).

[68] D. C. Ronquillo, A. Vengal, and N. Trivedi, Signatures of magnetic-field-driven quantum phase transitions in the entanglement entropy and spin dynamics of the Kitaev honeycomb model, Phys. Rev. B **99**, 140413 (2019).

[69] D. Takikawa and S. Fujimoto, Impact of off-diagonal exchange interactions on the Kitaev spin-liquid state of α-$RuCl_3$, Phys. Rev. B **99**, 224409 (2019).

[70] K. Hwang, A. Go, J. H. Seong, T. Shibauchi, and E.-G. Moon, Identification of a Kitaev quantum spin liquid by magnetic field angle dependence, Nat. Commun. **13**, 323 (2022).

[71] M. G. Yamada and S. Fujimoto, Quantum liquid crystals in the finite-field K-Γ model for α-$RuCl_3$, arXiv:2107.03045.

[72] H.-S. Kim, Y. B. Kim, and H.-Y. Kee, Revealing frustrated local moment model for pressurized hyperhoneycomb iridate: Paving the way toward a quantum spin liquid, Phys. Rev. B **94**, 245127 (2016).

[73] H.-Y. Lee, R. Kaneko, L. E. Chern, T. Okubo, Y. Yamaji, N. Kawashima, and Y. B. Kim, Magnetic field induced quantum phases in a tensor network study of Kitaev magnets, Nat. Commun. **11**, 1639 (2020).

[74] S. M. Winter, Y. Li, H. O. Jeschke, and R. Valentí, Challenges in design of Kitaev materials: Magnetic interactions from competing energy scales, Phys. Rev. B **93**, 214431 (2016).

[75] M. Gohlke, R. Moessner, and F. Pollmann, Dynamical and topological properties of the Kitaev model in a [111] magnetic field, Phys. Rev. B **98**, 014418 (2018).

[76] W. Wang, Z.-Y. Dong, S.-L. Yu, and J.-X. Li, Theoretical investigation of magnetic dynamics in α-$RuCl_3$, Phys. Rev. B **96**, 115103 (2017).

[77] S. M. Winter, K. Riedl, P. A. Maksimov, A. L. Chernyshev, A. Honecker, and R. Valentí, Breakdown of magnons in a strongly spin-orbital coupled magnet, Nat. Commun. **8**, 1152 (2017).

[78] J. Schmidt, D. D. Scherer, and A. M. Black-Schaffer, Topological superconductivity in the extended Kitaev-Heisenberg model, Phys. Rev. B **97**, 014504 (2018).

[79] R. Schaffer, S. Bhattacharjee, and Y. B. Kim, Quantum phase transition in Heisenberg-Kitaev model, Phys. Rev. B **86**, 224417 (2012).

[80] J. Yoshitake, J. Nasu, Y. Kato, and Y. Motome, Majorana dynamical mean-field study of spin dynamics at finite temperatures in the honeycomb Kitaev model, Phys. Rev. B **96**, 024438 (2017).

[81] C. Hickey and S. Trebst, Emergence of a field-driven U(1) spin liquid in the Kitaev honeycomb model, Nat. Commun. **10**, 530 (2019).

[82] T. Fukui, Y. Hatsugai, and H. Suzuki, Chern numbers in discretized Brillouin zone: Efficient method of computing (spin) Hall conductances, J. Phys. Soc. Jpn. **74**, 1674 (2005).

[83] For example the (h_1, h_3) and $(-h_1, -h_3)$ points are the same except for time-reversal symmetry (e.g., if ν is finite, then $\nu \to -\nu$).

[84] It should be noted that the conventions for the Chern number in Kitaev's original paper and the one used here differ in sign.

[85] We use Pauli matrix identities, e.g., $\sigma^z = i\sigma^x\sigma^y$ and replace σ^x with $-ib^yb^z$, etc., but not ib^xc.

[86] S.-S. Zhang, G. B. Halász, and C. D. Batista, Theory of the Kitaev model in a [111] magnetic field, Nat. Commun. **13**, 399 (2022).

[87] F. Yılmaz and M. Oktel, Hofstadter butterfly evolution in the space of two-dimensional Bravais lattices, Phys. Rev. A **95**, 063628 (2017).

[88] M.-H. Jiang, S. Liang, W. Chen, Y. Qi, J.-X. Li, and Q.-H. Wang, Tuning Topological Orders by a Conical Magnetic Field in the Kitaev Model, Phys. Rev. Lett. **125**, 177203 (2020).

[89] P. Saha, Z. Fan, D. Zhang, and G.-W. Chern, Hidden Plaquette Order in a Classical Spin Liquid Stabilized by Strong Off-Diagonal Exchange, Phys. Rev. Lett. **122**, 257204 (2019).

[90] J. Wang, B. Normand, and Z.-X. Liu, One Proximate Kitaev Spin Liquid in the K-J-Γ Model on the Honeycomb Lattice, Phys. Rev. Lett. **123**, 197201 (2019).

[91] I. Rousochatzakis and N. B. Perkins, Classical Spin Liquid Instability Driven By Off-Diagonal Exchange in Strong Spin-Orbit Magnets, Phys. Rev. Lett. **118**, 147204 (2017).

[92] A. M. Samarakoon, G. Wachtel, Y. Yamaji, D. A. Tennant, C. D. Batista, and Y. B. Kim, Classical and quantum spin dynamics of the honeycomb Γ model, Phys. Rev. B **98**, 045121 (2018).

[93] Q. Luo, J. Zhao, H.-Y. Kee, and X. Wang, Gapless quantum spin liquid in a honeycomb Γ magnet, npj Quantum Mater. **6**, 57 (2021).

[94] J. Chaloupka, G. Jackeli, and G. Khaliullin, Zigzag Magnetic Order in the Iridium Oxide Na_2IrO_3, Phys. Rev. Lett. **110**, 097204 (2013).

[95] J. Merino and A. Ralko, Majorana chiral spin liquid in a model for Mott insulating cuprates, Phys. Rev. Res. **4**, 023122 (2022).

[96] S. Trebst and C. Hickey, Kitaev materials, Phys. Rep. **950**, 1 (2022).

[97] K. A. Modic, R. D. McDonald, J. Ruff, M. D. Bachmann, Y. Lai, J. C. Palmstrom, D. Graf, M. K. Chan, F. Balakirev, J. Betts *et al.*, Scale-invariant magnetic anisotropy in $RuCl_3$ at high magnetic fields, Nat. Phys. **17**, 240 (2021).

[98] J. Wang, Q. Zhao, X. Wang, and Z.-X. Liu, Multinode quantum spin liquids on the honeycomb lattice, Phys. Rev. B **102**, 144427 (2020).

[99] X.-Y. Feng, G.-M. Zhang, and T. Xiang, Topological Characterization of Quantum Phase Transitions in a Spin-1/2 Model, Phys. Rev. Lett. **98**, 087204 (2007).